Effects of Fluid-Structure Interaction Modeling Assumptions on Seismic Floor Acceleration Demands within Gravity Dams

Najib Bouaanani [1] and Sylvain Renaud [2]

ABSTRACT

This paper presents an original investigation of the sensitivity of floor acceleration demands in gravity dams to various modeling assumptions of the impounded reservoir. Such floor acceleration demands are crucial for the assessment of the seismic performance or vulnerability of dam-supported appurtenant structures. Two approaches are proposed to obtain floor acceleration demands: analytical and coupled dam-reservoir finite element models. Both techniques are applied to typical dam-reservoir systems with different geometries. The dam-reservoir systems are subjected to ground motions with various frequency contents and the resulting floor acceleration demands are examined to investigate the effects of reservoir geometry, water compressibility, reservoir bottom wave absorption and dam higher vibration modes. A new approach based on proposed floor frequency response functions is also developed to assess floor acceleration demands at the stage of preliminary seismic design or safety evaluation of dam-supported appurtenant structures. Examples are given to illustrate how the proposed approach can be effectively used to compare floor acceleration demands within different dams or within the same dam considering various modeling assumptions of the reservoir.

Key words: Floor acceleration spectra; Appurtenant structures; Dam safety; Fluid-Structure interaction; Earthquake engineering; Finite elements; Added-mass formulation; Water compressibility.

[1] Professor, Department of Civil, Geological and Mining Engineering,
Polytechnique Montréal, Montréal, QC H3C 3A7, Canada
Corresponding author. E-mail: najib.bouaanani@polymtl.ca
[2] Graduate student, Department of Civil, Geological and Mining Engineering,
Polytechnique Montréal, Montréal, QC H3C 3A7, Canada

1 Introduction

Floor response spectra define maximum responses of light mass equipments or other secondary structures supported at various locations of a more massive primary structure. These spectra are commonly used to investigate the dynamic response of secondary structures when interaction with the primary structure can be neglected. Floor response spectra were extensively studied in the contexts of nuclear facilities and multi-storey buildings (Singh 1975; Singh 1980; Singh 1985; Asfura and Der Kiureghian 1986; Chen and Soong 1988). Floor response spectra can also be used to assess the dynamic response of safety-critical piping, power supply units, and other electrical or mechanical equipment anchored within dam galleries as well as appurtenant facilities such as bridges, control unit buildings, spillway support structures, gates, hoist bridges and lifting equipment generally located near dam crest where ground motions can be significantly amplified from dam base. For example, seismic records at three dam sites in Quebec during the Saguenay earthquake showed motion amplifications of 7 to 15 times from rock to dam crest (Rainer and Dascal 1991).

Assessment of maximum floor acceleration demands along the height of hydraulic structures is crucial for the design and safety evaluation of appurtenant systems. Indeed, amplification of seismic demands in dams may cause significant damage as was documented in several cases, such as the 103 m-high Koyna dam (India) after the 1967 M6.3 reservoir induced earthquake, the 105 m-high Hsingfengkiang buttress dam (China) under the effect of a 1962 M6.1 reservoir induced earthquake, and the 106 m-high Sefid-Rud buttress dam (Iran) following a 1990 M7.3 earthquake (Hansen and Roehm 1979, Arcangeli and Ciabarri 1994, ICOLD 2001). In other events, if damage to the dam itself remained marginal, supported equipment and appurtenant structures were severely affected by amplified ground motions which induced offset or cracking of elements such as walls, parapets, or bridge girders (USCOLD 2000, Matsumoto et al. 2011). Amplifications of seismic demands in dams were also evidenced by shake table tests (Donlon and Hall 1991, Lin et al. 1993, Tinawi et al. 2000). Therefore, modern guidelines dealing with the earthquake response of dams, such as ICOLD (2010), clearly specify that seismic input at the support of equipments or at the base of appurtenant structures should take account of ground motion amplifications. Such practice has not been always uniformly observed however, especially for older dams and appurtenant structures with initial designs that may fail to meet modern safety criteria.

Weiland and Malla (2000) performed 3D dynamic analysis of a 45 m-high arch-gravity dam assuming that water in the reservoir is incompressible. They found an acceleration amplification factor with respect to the PGA of 3.8 at the upper gallery, and about 8 at dam crest. They also used the floor response spectrum at a given level to generate artificial spectrum-compatible accelerograms used to conduct stability analyses of an upper cracked portion of the dam (Wieland and Malla 2000; Malla and Wieland 2003). Ben Ftima and Léger (2006) investigated the possibility to compute floor response spectra at the base of cracked sections of a gravity dam and the use of these spectra to define compatible accelerograms to perform transient rigid body sliding/rocking response analyses along dam's height. They used Westergaard's added masses to represent hydrodynamic loads from the reservoir.

It is now widely accepted that the accurate evaluation of reservoir loading on a dam upstream face is an important ingredient of its seismic safety assessment. Significant research has been devoted to study this type of loading since the pioneering work of Westergaard (1933). Several advanced analytical and numerical frequency-domain and time-domain approaches were also proposed to account for dam deformability, water compressibility, radiation of outgoing waves towards far reservoir upstream, and reservoir bottom wave absorption in the seismic response of dam-reservoir systems, such as described for example by Chopra (1970), Fenves and Chopra (1984), Humar and Jablonski (1988), and Bouaanani and Lu (2009). To the authors knowledge however, no published work has addressed the sensitivity of floor acceleration demands to modeling assumptions commonly adopted for hydraulic structures such as gravity dams, namely those related to hydrodynamic loading. These assumptions may range from simplified added mass approach to more advanced treatment of frequency-dependent dam-reservoir interaction, including water compressibility, reservoir bottom wave absorption and energy dissipation at far reservoir upstream. Dam engineering analysts are usually left to select the most appropriate of these assumptions for a particular project without having sens or prior knowledge of the relative impacts on the design or safety evaluation of appurtenant infrastructure. Informed choices are however crucial considering the critical importance and seismic vulnerability that may be associated with dam-supported appurtenant structures. This paper's main objective is to feed such informed choices as analytical and coupled dam-reservoir finite element models are proposed and used to thoroughly investigate the effects of various assumptions on floor acceleration demands within typical dam-reservoir systems with different geometries.

2   Basic notation and types of analyses

2.1   Floor acceleration demands

We consider a gravity dam monolith, of height H_d, subjected to a horizontal ground acceleration $\ddot{u}_g$ at the base as illustrated in Fig. 1. Floor seismic demands at a given point P of the dam are defined by studying the dynamic response of SDOF systems with various vibration frequencies f_s, attached to point P, while the dam is excited by a ground acceleration $\ddot{u}_g$ applied at its base. These SDOF systems, may represent dam-supported appurtenant secondary structures, with mass m_s, stiffness k_s and viscous damping c_s. We assume that the mass of the appurtenant secondary SDOF system is too light so that its dynamic response does not affect that of the primary system, i.e. the dam monolith. The equation of motion of the appurtenant SDOF can be written as

$$m_s\ddot{u}_s + c_s\dot{u}_s + k_su_s = -m_s(\ddot{u}_P + \ddot{u}_g) \tag{1}$$

where $\ddot{u}_P$ denotes the horizontal acceleration at point P of the dam relative to its base, and u_s, $\dot{u}_s$ and $\ddot{u}_s$ the horizontal displacement, horizontal velocity and horizontal acceleration of the secondary SDOF system relative to point P, respectively.

The floor acceleration demand $\Gamma(y_P)$, at a point P of coordinate y_P, is defined hereafter as the maximum

absolute acceleration response $\left|\ddot{u}_{\mathrm{s}} + \ddot{u}_{\mathrm{P}} + \ddot{u}_{\mathrm{g}}\right|$ of the secondary SDOF system for a given vibration frequency $f_{\mathrm{s}} = \dfrac{1}{2\pi}\sqrt{\dfrac{k_{\mathrm{s}}}{m_{\mathrm{s}}}}$ and damping coefficient c_{s} or equivalent damping ratio $\xi_{\mathrm{s}} = \dfrac{c_{\mathrm{s}}}{4\pi m_{\mathrm{s}} f_{\mathrm{s}}}$. We denote by $\Gamma^{*}(y_{\mathrm{P}})$ the maximum or peak floor acceleration at a point P of coordinate y_{P} over the whole range of frequencies f_{s} considered. Solving Eq. (1) requires the determination of the acceleration $\ddot{u}_{\mathrm{P}}$ at point P relative to the dam base. This can be achieved using a coupled dam-reservoir finite element model or a semi-infinite reservoir analytical model as described in the next two sections.

2.2 Coupled dam-reservoir finite element model

The floor acceleration demands in a gravity dam can be obtained using a coupled dam-reservoir finite element model as the one illustrated in Fig. 1 (a). In this case, the dam and the reservoir are modeled using solid plane elasticity and potential-based fluid finite elements, respectively. The reservoir is truncated at a certain distance L_{r} from the dam upstream face, large enough to eliminate reflection of waves at the far reservoir upstream end. Fluid-structure interaction is accounted for through special elements at the dam-reservoir interface. Dam vibrations cause water motions normal to its boundaries, and the induced-pressure within water cause additional hydrodynamic loads to act on the dam. In the present case of two-dimensional analysis, the fluid-structure interface elements are 2-node line segments, which connect 4-node solid elements on the upstream face of the gravity dam to adjacent potential-based fluid elements on the reservoir boundary. Each node of the interface element contains a potential degree of freedom and two horizontal and vertical structural displacement degrees of freedom. The potential and structural degrees of freedom are related through a compatibility boundary condition.

The procedure used to obtain the seismic response of the dam, such as accelerations, is known as the $\phi - U$ formulation since it is expressed in terms of displacements U and velocity potentials ϕ as state variables in the solid and water domains, respectively. It is assumed that the fluid is inviscid, compressible or incompressible, and with an irrotational motion and relatively small displacements of the fluid-structure boundaries. Details of the $\phi - U$ formulation can be found elsewhere (Everstine 1981, Olson and Bathe 1985a, Olson and Bathe 1985b, Bouaanani and Lu 2009) and only a brief review is given hereafter for convenient reference. Under the above assumptions, the velocity potential ϕ in the reservoir satisfies the wave equation

$$\nabla^{2}\phi = \frac{1}{C_{\mathrm{r}}^{2}}\frac{\partial^{2}\phi}{\partial t^{2}} \tag{2}$$

where C_{r} is the velocity of compression waves within water, and t the time variable. The velocity potential ϕ satisfies a free surface boundary condition, a compatibility boundary condition at the vibrating dam-reservoir interface (Fenves and Chopra 1984, Bouaanani and Lu 2009), a radiation boundary condition to prevent reflection of waves at the far upstream of the reservoir (Sommerfeld 1949, Zienkiewicz and Newton 1969, Bouaanani and Lu 2009, ADINA 2011), and a boundary condition accounting for energy dissipation at reservoir bottom through one-dimensional partial wave absorption of incident compression waves normal to the reservoir-foundation interface (Hall and Chopra 1982, Fenves and Chopra 1984,

4

Bouaanani and Lu 2009). The last two boundary conditions can be modeled by infinite fluid elements placed at the upstream end of the reservoir and by viscous dampers placed at reservoir bottom, as will be illustrated later.

Using standard techniques, the weak variational form of Eq. (2) can be obtained and discretized to yield the following system of equations (Zienkiewicz and Newton 1969; Olson and Bathe 1985a)

$$
\begin{bmatrix} \mathbf{M}_{\mathrm{dd}} & \mathbf{0} \\ \mathbf{0} & -\mathbf{M}_{\mathrm{rr}} \end{bmatrix} \begin{bmatrix} \ddot{\mathbf{U}} \\ \ddot{\boldsymbol{\Phi}} \end{bmatrix} + \begin{bmatrix} \mathbf{C}_{\mathrm{dd}} & \mathbf{C}_{\mathrm{rd}}^{\mathrm{T}} \\ \mathbf{C}_{\mathrm{rd}} & \mathbf{C}_{\mathrm{rr}} \end{bmatrix} \begin{bmatrix} \dot{\mathbf{U}} \\ \dot{\boldsymbol{\Phi}} \end{bmatrix} + \begin{bmatrix} \mathbf{K}_{\mathrm{dd}} & \mathbf{0} \\ \mathbf{0} & -\mathbf{K}_{\mathrm{rr}} \end{bmatrix} \begin{bmatrix} \mathbf{U} \\ \boldsymbol{\Phi} \end{bmatrix} = \begin{bmatrix} -\mathbf{M}_{\mathrm{dd}}\, \mathbf{1}\, \ddot{u}_{\mathrm{g}} \\ -\mathbf{C}_{\mathrm{rd}}\, \mathbf{1}\, \dot{u}_{\mathrm{g}} \end{bmatrix} \tag{3}
$$

where $\mathbf{U}$ and $\boldsymbol{\Phi}$ are vectors containing nodal relative displacements and fluid potentials, $\mathbf{M}_{\mathrm{dd}}$ and $\mathbf{K}_{\mathrm{dd}}$ are the structural mass and stiffness matrices of the dam, respectively, $\mathbf{C}_{\mathrm{dd}}$ is a damping matrix of the dam structure that can be determined using a Rayleigh damping, equivalent to a modal damping ξ_{d} or hysteretic damping η_{d}, $\mathbf{M}_{\mathrm{rr}}$ and $\mathbf{K}_{\mathrm{rr}}$ are the potential and kinetic energy matrices of the impounded reservoir, respectively, $\mathbf{C}_{\mathrm{rd}}$ is a matrix coupling the velocity potential to displacements on the dam-reservoir interface, matrix $\mathbf{C}_{\mathrm{rr}}$ accounts for damping due to energy dissipation at the reservoir bottom or at the far upstream boundary of the reservoir, $\ddot{u}_{\mathrm{g}}$ and $\dot{u}_{\mathrm{g}}$ are prescribed ground accelerations and velocities, and $\mathbf{1}$ is a column vector with the same dimension as $\mathbf{U}$, containing ones when a translational degree of freedom corresponds to the direction of earthquake excitation, and zero otherwise. The solution of Eq. (3) provides the time-history response of the dam, including accelerations $\ddot{u}_{\mathrm{P}}$ at any point P to which an appurtenant secondary structure might be attached.

2.3 Semi-infinite reservoir analytical model

According to this technique, only the dam monolith is modeled using finite elements, while the effect of impounded reservoir is modeled analytically. In this case, the reservoir is assumed of rectangular shape with height H_{r} as illustrated in Fig. 1 (b). Time-history acceleration response $\ddot{u}_{\mathrm{P}}$ at a given point P to ground motion $\ddot{u}_{\mathrm{g}}$ can then be obtained at each time t as (Fenves and Chopra 1984, Bouaanani and Lu 2009)

$$
\ddot{u}_{\mathrm{P}}(t) = \sum_{j=1}^{N_{\mathrm{d}}} \psi_j^{(x)}(x_{\mathrm{P}}, y_{\mathrm{P}})\, \ddot{Z}_j(t) \tag{4}
$$

where N_{d} is the number of dam structural mode shapes included in the analysis, $\psi_j^{(x)}$ is the x–components of the $j^{\,\mathrm{th}}$ dam mode shape, taken at the coordinates $(x_{\mathrm{P}}, y_{\mathrm{P}})$ of point P, and $\ddot{Z}_j$ is the second time-derivative of generalized coordinates given by the Fourier integral

$$
\ddot{Z}_j(t) = -\frac{1}{2\pi} \int_{-\infty}^{\infty} \omega^2 \bar{Z}_j(\omega)\, \bar{\ddot{u}}_{\mathrm{g}}(\omega)\, \mathrm{e}^{\mathrm{i}\omega t}\, \mathrm{d}\omega \tag{5}
$$

in which $\bar{\ddot{u}}_{\mathrm{g}}(\omega)$ is the Fourier transform of the ground acceleration $\ddot{u}_{\mathrm{g}}(t)$

$$
\bar{\ddot{u}}_{\mathrm{g}}(\omega) = \int_0^{t_a} \ddot{u}_{\mathrm{g}}(t)\, \mathrm{e}^{-\mathrm{i}\omega t}\, \mathrm{d}t \tag{6}
$$

5

with t_a denoting the time duration of the applied accelerogram. The vector $\bar{\mathbf{Z}}$ of generalized coordinates $\bar{Z}_j$, $j=1\ldots N_\mathrm{d}$, required in Eq. (5) can be obtained by solving the system of equations

$$\bar{\mathbf{S}}\,\bar{\mathbf{Z}} = \bar{\mathbf{Q}} \tag{7}$$

where, for $n=1\ldots N_\mathrm{d}$ and $j=1\ldots N_\mathrm{d}$

$$\bar{S}_{nj}(\omega) = \left[-\omega^2 + \left(1 + \mathrm{i}\,\eta_\mathrm{d}\right)\omega_n^2 \right]\delta_{nj} + \omega^2 \int_0^{H_\mathrm{r}} \bar{p}_j(0,y,\omega)\,\psi_n^{(x)}(0,y)\,\mathrm{d}y \tag{8}$$

$$\bar{Q}_n(\omega) = -\boldsymbol{\psi}_n^\mathrm{T}\,\mathbf{M}_\mathrm{dd}\,\mathbf{1} + \int_0^{H_\mathrm{r}} \bar{p}_0(0,y,\omega)\,\psi_n^{(x)}(0,y)\,\mathrm{d}y \tag{9}$$

in which δ_{nj} denotes the Kronecker symbol, ω the exciting frequency, η_d the dam hysteretic damping factor assumed constant, ω_n the vibration frequency corresponding to structural mode shape $\boldsymbol{\psi}_n$ of the dam with empty reservoir, $\bar{p}_0$ the frequency response function (FRF) for hydrodynamic pressure at rigid dam upstream face due to ground acceleration, $\bar{p}_j$ the FRF for hydrodynamic pressure due to horizontal acceleration $\psi_j^{(x)}(0,y)$ of the dam upstream face, and H_r the constant height of the rectangular reservoir. The hydrodynamic pressures are determined analytically, by solving the Helmholtz equation and associated boundary conditions accounting for: (i) a free surface boundary condition, (ii) a fluid-structure boundary condition implying compatibility between hydrodynamic pressures and normal displacements at dam-reservoir interface, (iii) a radiation boundary condition upstream of the reservoir to simulate non reflection of outgoing waves at infinity, and (iv) a boundary condition at reservoir bottom to approximately account for energy dissipation due to sedimentation through one-dimensional partial wave absorption of incident compression waves, characterized by a reflection coefficient α varying from $\alpha=0$ for full absorption, to $\alpha = 1$ for full reflection. Details of the calculations of hydrodynamic pressures are not reviewed here for brevity and can be found elsewhere (Fenves and Chopra 1984, Bouaanani and Lu 2009). A convergence study has to be conducted to determine the sufficient numbers N_d of structural mode shapes to be included. Such analysis will be performed later to evaluate the effect on floor acceleration spectra.

3   Case studies, results and discussions

3.1   Dam-reservoir systems considered

The methods presented above are applied next to investigate the sensitivity of floor acceleration demands in two typical dam-reservoir systems considering various modeling assumptions. Two gravity dams with heights of $35\,\mathrm{m}$ and $90\,\mathrm{m}$ are studied to assess dam size effects on floor acceleration demands. For brevity of notation, the $35\,\mathrm{m}$- and $90\,\mathrm{m}$-high gravity dams are designated, respectively, by D1 and D2 hereafter. For each dam, rectangular and irregular reservoir geometries are considered as illustrated in Figs. 2 and 3. A modulus of elasticity $E_\mathrm{d}=25\,\mathrm{GPa}$, a Poisson's ratio $\nu_\mathrm{d}=0.2$, and a density $\rho_\mathrm{d}=2400\,\mathrm{kg/m}^3$ are adopted as concrete material properties. Compressible water in the impounded reservoir is modeled using a mass density $\rho_\mathrm{r}=1000\,\mathrm{kg/m}^3$ and a bulk modulus $\mu_\mathrm{r}=2.07\times10^3\,\mathrm{MPa}$ corresponding to a velocity of pressure

waves $C_r = 1440$ m/s. A very large bulk modulus is considered to remove water compressibility effects for comparison purposes.

The finite element software ADINA (2011) is used to build the coupled dam-reservoir finite element models described in Section 2.2. This software implements the $\phi - U$ described previously, and was validated elsewhere against analytical and experimental results from dynamic fluid-structure interaction problems in civil engineering (Bouaanani and Lu 2009, Bouaanani et al. 2012, Wei et al. 2013). The dam-reservoir mesh consists mainly of 9-node plane stress solid and potential-based fluid finite elements, with some 7-node triangular transition elements in the reservoir. Special infinite fluid elements based on the plane-wave and doubly asymptotic approximations are placed at a truncation distance L_r from dam face to simulate infinite fluid region upstream of the reservoir (Olson and Bathe 1985b, Hamdan and Dowling 1995, ADINA 2011). The effect of reservoir truncation length on floor acceleration demands will be discussed later. Energy dissipation due to sedimentation can be simulated by considering a series of axially vibrating thin independent columns of infinite lengths, extending in the direction normal to reservoir bottom (Hall and Chopra 1982, Fenves and Chopra 1984). Using this analogy and the technique proposed by Lysmer and Kuhlemeyer (1969), we show that the absorptive condition at reservoir bottom can be approximated by a series of viscous dampers placed in the direction normal to reservoir bottom (Bouaanani and Lu 2009). These viscous dampers are illustrated in Figs. 2 and 3. To ensure compatibility between fluid and damper elements and enable fluid-structure interaction, isoparametric beam elements, with negligible mass and stiffness properties are inserted along reservoir-foundation interface. 2-node damper elements are then built by connecting beam element nodes to the ground. Damper and beam element nodes are constrained to move only perpendicularly to the reservoir bottom boundary. We show that the consistent vector of damping coefficients $\mathbf{c}^{(e)}$ corresponding to each beam element e with length $\ell^{(e)}$ can be expressed in terms of mass density ρ_r, velocity of compression waves C_r and reflection coefficient α as

$$\mathbf{c}^{(e)} = \rho_r C_r \left(\frac{1 + \alpha}{1 - \alpha} \right) \int_{-1}^{1} \mathbf{N}_b^{\mathrm{T}} \, \mathrm{d}r \tag{10}$$

where $\mathbf{N}_b$ denotes the isoparametric shape function of the beam element and r the isoparametric coordinate. Figs. 2 (a) and 3 (a) illustrate the determination of viscous damping values for the 3-node beam elements used in this work. A Rayleigh damping equivalent to a modal damping $\xi_d = 5\%$ of the dam is adopted. As seen previously, the right hand side of Eq. (3) accounts for earthquake loading through prescribed ground accelerations $\ddot{u}_g$ and velocities $\dot{u}_g$. This loading can be introduced either as mass-proportional body forces when ground motions are applied uniformly to the dam-reservoir system, or as prescribed ground displacements when variability of seismic input is of concern (Bouaanani and Lu 2009). In this work, mass-proportional body forces are adopted. The ground velocities $\dot{u}_g$ are obtained from input ground accelerations by numerical integration. An implicit Newmark integration scheme is used and the time step adopted for each analysis is based on convergence studies.

The analytical method described in Section 2.3 is programmed to obtain floor acceleration demands in any point of the gravity dams. The software ADINA (2011) is used to discretize the dry dams into

7

9-node plane stress finite elements to obtain the mode shapes, natural frequencies and corresponding modal participation factors. The same mesh densities of the dams in the coupled finite element models are used. We consider a dam hysteretic damping factor $\eta_d = 0.1$, which is equivalent to a modal viscous damping ratio $\xi_d = 5\%$. The analytical method is used later to evaluate the effect of the number of included structural modes on floor acceleration demands.

The floor acceleration demands within each dam-reservoir system are determined under the effect of various seismic inputs described in the next section. Seismic demands within the dams with empty reservoirs are also given for comparison purposes. All floor acceleration spectra are determined considering a viscous damping $\xi_s = 5\%$ of the appurtenant secondary structures. For practical discussion of the results hereafter, we refer to a dam with an empty reservoir as a dry structure, and as wet structure otherwise.

3.2   Earthquake loading

Four ground motions with acceleration time-histories and acceleration spectra illustrated in Fig. 4 are considered in this work: (i) a horizontal component of Imperial Valley earthquake (1940) at station El Centro, (ii) a horizontal component of Parkfield earthquake (1966) at station Cholame no. 5, (iii) a horizontal component of Loma Prieta earthquake (1989) at station Gilroy Array no. 2, and (iv) a horizontal component of Saguenay earthquake (1988) at station La Malbaie. The first three records were obtained from PEER ground motion database (PEER 2012), and the forth from the Geological Survey of Canada (GSC 2006). The four ground motions were selected considering the differences in their time-history traces as well as frequency content as shown in Fig. 4. The effect of these variations on floor acceleration demands within dams D1 and D2 will be discussed in what follows.

3.3   Effect of reservoir truncation length

Finite element discretization of a semi-infinite rectangular reservoir requires its truncation at a finite length and application of an appropriate boundary condition that accounts for energy dissipation at the far upstream end. In this work, special infinite fluid finite elements provided in ADINA (2011) are used. It is important to investigate the effect of truncation length on the convergence of the results. For this purpose, special fluid elements are applied at three increasing truncation distances from dam face: $L_r = 2H_r$; $L_r = 4H_r$ and $L_r = 20H_r$. Fig. 5 illustrates the floor acceleration demands $\Gamma(H_d)$ obtained at the crests of dams D1 and D2 (Point A in Figs. 2 and 3) subjected to Imperial Valley ground motion considering the previously defined truncation lengths and a fully reflective reservoir bottom, i.e. $\alpha = 1$. The floor accelerations are non-dimensionalized with respect to the PGA of the applied ground motion. It can be seen that convergence of the results is ensured using a truncation length $L_r = 4H_r$.

To investigate convergence sensitivity to the location where floor acceleration demands are computed, these demands are determined as point P moves along the dam cross-section's middle line made of two segments relating points A, B and C as indicated in Figs. 2 and 3. Fig. 6 illustrates the profiles of max-

imum floor acceleration demands $\Gamma^*(y_P)$, $0 \leqslant y_P \leqslant H_d$, when the dams are subjected to Imperial Valley ground motion, considering the three truncation lengths defined previously. Peak floor accelerations are non-dimensionalized with respect to the PGA of the applied ground motions to get a sense of the induced amplifications. The results in Fig. 6 confirm that a truncation length of $L_r = 4H_r$ gives a good compromise between accuracy and efficient numerical computation. The same conclusion is also reached considering the other ground motions described under Section 3.2. Hence, only results using this truncation length are presented and discussed in the rest of the paper. This corresponds to rectangular and irregular reservoirs truncated at a distance $L_r = 128$ m and $L_r = 344$ m from D1 and D2 dam faces, respectively.

3.4   Effect of reservoir geometry

In this section, we investigate the effect of reservoir geometry on floor acceleration demands within the studied dams. For this purpose, we consider the irregular reservoir geometries shown in Figs. 2 (b) and 3 (b). We note that the same truncation length $L_r = 4H_r$ is considered for the rectangular and irregular reservoir geometries for comparison purposes. Dams D1 and D2 are then subjected to the Imperial Valley, Parkfield, Loma Prieta, and Saguenay ground motions described previously. The resulting floor acceleration demands at the crests of dams D1 and D2 impounding rectangular and irregular geometry reservoirs are depicted in Fig. 7. The acceleration demands at the crest of the dry structures are also shown for comparison purposes. This comparison shows that fluid-structure interaction effects are generally significant in the evaluation of floor acceleration demands of both dams. For both reservoir geometries, we observe that hydrodynamic loads can be neglected up to a frequency varying from approximately 1.5 Hz for dam D2 subjected to Imperial Valley ground motion to approximately 4 Hz for dams D1 and D2 subjected to Saguenay ground motion. After this frequency range, fluid-structure interaction alters floor acceleration demands either in terms of amplitudes or frequency content. Referring to acceleration spectra in Figs. 4 (b) and (h), it can be seen that the values of 1.5 Hz and 4 Hz correspond roughly to the start of predominant frequencies of Imperial Valley and Saguenay earthquakes, respectively. The results in Fig. 7 globally show that, for the cases studied, the more rigid is the dam-supported appurtenant structure, the more its dynamic response is affected by fluid-structure interaction. We also observe that fluid-structure interaction can lead to amplification or reduction of floor acceleration demands with respect to the empty reservoir case. This interesting result shows that, in some situations, maximum floor acceleration demands can be associated with an empty reservoir, and can then be obtained without reservoir modeling and fluid-structure interaction analyses.

Fig. 7 also reveals that the influence of reservoir geometry is negligible over the whole studied frequency range for dam D1 when shaken by Parkfield earthquake, and only up to a frequency of about 15 Hz when the other ground motions are applied. After this frequency, the irregular reservoir is generally associated with larger floor acceleration demands at the crest of dam D1. Most important differences between floor accelerations corresponding to both types of reservoirs are however concentrated between 15 Hz and 25 Hz approximately. Examination of the response of dam D2 shows that reservoir geometry does not affect crest floor acceleration demands for frequencies up to about 5 Hz for all applied ground mo-

9

tions. After this frequency, the irregular reservoir corresponds to higher acceleration amplitudes up to a frequency of about $22\,\mathrm{Hz}$ under the effect of Saguenay ground motion, and over the whole frequency range for all other applied ground motions.

The previous results focused on the frequency evolution of seismic floor accelerations at the crest of dams D1 and D2. Non-dimensionalized maximum floor acceleration demands $\Gamma^*(y_\mathrm{P})/\mathrm{PGA}$ along the height of the two dams are also illustrated in Fig. 8. It is clearly seen that maximum floor acceleration profiles are very sensitive to the geometry of the dam studied and applied earthquake. For dam D1, the lowest maximum floor accelerations are obtained for the dry structure under the effect of all considered earthquakes. Maximum differences with responses of the wet structure are produced by Parkfield and Saguenay ground motions, yielding amplifications with respect to the dry case of about 130% and 65%, respectively. For dam D2, the dry structure develops the highest floor accelerations near the crest for all studied earthquakes. Below this location, the differences between maximum floor acceleration demands in the dry and wet structures vary depending on the earthquake applied as illustrated in Figs. 8 (b), (d), (f) and (h). Largest floor acceleration demands for dam D2 are obtained within the dry structure under the effect of Saguenay earthquake, and within the wet structure when subjected to Imperial Valley and Parkfield ground motions. Imperial Valley and Loma Prieta earthquakes induce the least differences between maximum floor acceleration demands within dry and wet dam D2. We also observe from Fig. 8 that reservoir geometry has generally little effect on maximum floor acceleration demands in both dams. Maximum differences between results corresponding to rectangular and irregular reservoirs are found at the crest, with the largest being observed at the crest of dam D2 under the effect of Imperial Valley ground motion.

3.5 Effects of reservoir bottom wave absorption

The sensitivity of floor accelerations at the crest of dams D1 and D2 to reservoir bottom wave absorption is illustrated in Figs. 9 and 10, respectively. The dams impound rectangular and irregular reservoirs characterized by bottom reflection coefficients of $\alpha = 1.0$, $\alpha = 0.8$, $\alpha = 0.6$, $\alpha = 0.4$ and $\alpha = 0.2$ and are subjected to the Imperial Valley, Parkfield, Loma Prieta, and Saguenay ground motions as previously. The floor accelerations within the dry structures are also shown for comparison purposes. The results depicted in Fig. 9 indicate that maximum effects of energy dissipation at reservoir bottom are generally concentrated around the main resonant segments of the curves, i.e. near 8 to $10\,\mathrm{Hz}$. We observe that floor acceleration demands at the crest of dam D1 increase as reservoir bottom wave absorption is lower, with the full reflection case, i.e. $\alpha = 1.0$, being generally notably distinct from the other absorption levels. Practically the same observations apply to the floor accelerations at the crest of dam D2 subjected to Imperial Valley and Parkfield earthquakes as illustrated by Figs. 10 (a) to (d). However, the floor accelerations corresponding to Loma Prieta and Saguenay earthquakes do not follow the same trends as revealed by Figs. 10 (e) to (h). For example, floor acceleration demands at the crest of dam D2 subjected to Saguenay ground motion are found to decrease with reservoir bottom wave absorption contrary to what was observed previously. For both dams, the effect of reservoir geometry could be neglected except for the

fully reflective case, i.e. $\alpha = 1.0$. This effect is observed at frequencies higher than approximately $15\,\mathrm{Hz}$ for dam D1. The same effect is less definite for dam D2, except when subjected to Imperial Valley earthquake and for frequencies up to $20\,\mathrm{Hz}$. Overall, it can be concluded that reservoir geometry effects are attenuated as energy dissipation is increased due to higher reservoir bottom wave absorption.

Figs. 11 and 12 show the profiles of non-dimensionalized maximum floor acceleration demands $\Gamma^*(y_\mathrm{P})/\mathrm{PGA}$ along the heights of dams D1 and D2, respectively. It is seen that maximum floor accelerations increase with lower reservoir bottom wave absorption for dam D1, and that the lowest peak floor accelerations correspond to the empty reservoir. However, the dispersion of the profiles depends on the earthquake applied, varying from very close for Imperial Valley and Loma Prieta ground motions, to more separated for Parkfield and Saguenay ground motions. Maximum amplifications for dam D1 vary from about 10 under the effect of Loma Prieta ground motion to about 27 under the action of Saguenay ground motion. These amplifications are slightly higher for the rectangular reservoir. Fig. 12 shows that the profiles of maximum floor acceleration demands within dam D2 present different features. First, maximum amplifications under the effect of Imperial Valley earthquake are almost identical for all reservoir bottom absorption levels except the fully reflective case. We also observe that maximum floor accelerations increase with lower reservoir bottom wave absorption under the effect of Loma Prieta earthquake, while this trend does not apply for Parkfield and Saguenay earthquakes.

3.6 Effects of water compressibility

The previous results were obtained assuming that water in the reservoir is compressible. In this section, we investigate the effect of this assumption by comparing the results to cases: (i) where the water in the reservoir is assumed incompressible by considering a very large bulk modulus as explained in Section 3.1, and (ii) where hydrodynamic loads are modeled using Westergaard's added mass formulation (Westergaard 1933). According to the latter formulation, the effect of the reservoir is equivalent to inertia forces generated by a body of water of parabolic shape moving back and forth with the vibrating dam which is assumed rigid. The Westergaard added mass $m_i^{(\mathrm{W})}$ to be attached to a node i belonging to dam-reservoir interface can be obtained as

$$m_i^{(\mathrm{W})} = \frac{7}{8}\,\rho_\mathrm{r}\,S_i\,\sqrt{H_\mathrm{r}\left(H_\mathrm{r} - y_i\right)} \tag{11}$$

where y_i denotes the height above the dam's base of node i of the dam-reservoir interface and S_i the transverse surface area associated to node i, considering a unit-thick slice of the studied gravity dam. The same 9-node finite element discretizations described previously for dams D1 and D2 are used and a consistent formulation is applied to evaluate the added masses.

Figs. 13 to 16 compare the results obtained using incompressible water assumption and added mass formulation to those corresponding to a fully reflective reservoir containing compressible water. The responses of the dry structures are also plotted for comparison purposes. These figures clearly show the high sensitivity of floor acceleration demands to above-mentioned reservoir modeling assumptions, and illustrate that water compressibility affects the dynamic response of appurtenant secondary structures

differently depending on the dam and frequency ranges considered. It is first seen that reservoir geometry has practically no effect on the floor acceleration demands corresponding to the incompressible water assumption, as opposed to the higher sensitivity associated with energy radiation in the reservoir due to water compressibility. The incompressible water assumption induces the highest floor acceleration demands at the crest of dam D1 subjected to Imperial Valley and Loma Prieta earthquakes and the crest of dam D2 subjected to Loma Prieta and Parkfield earthquakes. The added mass formulation leads to the largest peak floor accelerations at the crest of dam D1 subjected to Saguenay ground motion, and at the crest of dam D2 subjected to Imperial Valley and Saguenay ground motions. Floor accelerations corresponding to the compressible water assumption are the largest only for dam D1 subjected to Parkfield and Saguenay earthquakes. The floor acceleration spectra at dam crest corresponding to the three assumptions are practically identical in the lower frequency range up to about $8\,\mathrm{Hz}$ for dam D1 and about $3\,\mathrm{Hz}$ for more flexible dam D2. At higher frequencies, floor acceleration demands corresponding to incompressible water assumption and added mass formulation are generally closer, as dam flexibility effects diminish. The profiles of maximum floor acceleration demands confirm the sensitivity of the responses to reservoir modeling assumptions, with differences generally decreasing as the position where seismic demand is computed is lower. The largest difference between the results corresponding to compressible and incompressible water assumptions is obtained at the crest of dam D2 subjected to Saguenay earthquake as illustrated in Figs. 16 (g) or (h).

3.7 Effects of higher vibration modes of the dry structure

The simplified procedure presented in Section 2.3 is applied next to assess the number N_d of structural modes to be included in analysis on floor acceleration demands. Figs. 17 to 20 show the obtained results for $N_\mathrm{d} = 1$, $N_\mathrm{d} = 3$, $N_\mathrm{d} = 5$ and $N_\mathrm{d} = 7$. The cases of the dry dams are also presented to illustrate the effect of dam-reservoir interaction including water compressibility on the results. It is clearly seen that the number of modes to be included in the analysis depends on the flexibility of the dam and the predominant frequency range of the appurtenant secondary structure considered. For example, for the dry dam D1, the results show that: (i) the fundamental mode is required to obtain floor acceleration demands at frequencies up to about $15\,\mathrm{Hz}$ for all earthquakes, and (ii) two modes are required to cover the whole frequency range for all earthquakes except Saguenay ground motion, which necessitates including five structural modes in the high frequency range, although the error introduced otherwise is negligible as can be seen from Fig. 17 (g). The same observations apply for the wet dam D1, with the difference that the error introduced by considering less that required structural modes is slightly attenuated with respect to the dry case. Fig. 18 shows that a fundamental mode analysis is sufficient to assess maximum floor acceleration demands $\Gamma^*(y_\mathrm{P})$ as they occur at low frequencies less than $15\,\mathrm{Hz}$ for dam D1. For higher dam D2, we observe, as expected, that more modes are required to obtain convergence of floor acceleration demands for the same frequency range. For instance, fundamental mode response is valid only for a frequency range up to $5\,\mathrm{Hz}$, while 5 modes are needed to cover the whole frequency range considered as shown in Fig. 19. It is also seen that in this case, fundamental mode analysis can lead to inaccurate maximum floor

acceleration demands $\Gamma^*(y_P)$ as for the dry dam subjected to Imperial Valley and Parkfield earthquakes, i.e. Figs. 20 (a) and (c), or the wet structure subjected to Saguenay ground motion, i.e. Fig. 20 (h).

3.8 Proposed Floor Frequency Response Functions

The results presented previously were obtained under the effects of four earthquakes with various time-history traces and frequency contents. We illustrated that some observed behaviors are complex and cannot be interpreted easily based simply on the frequency contents of the earthquakes and natural frequencies of the dam and appurtenant structures. For preliminary design and safety evaluation purposes, it is generally worth carrying out a harmonic analysis to compare floor acceleration demands within different dams or the same dam considering various assumptions. In this section, we propose a new approach for assessing floor acceleration demands under the effect of unit horizontal harmonic ground acceleration $\ddot{u}_g(t) = \mathrm{e}^{\mathrm{i}\omega t}$, where ω is the exciting frequency. For this purpose, we introduce a floor frequency response function (FFRF) which defines the relationship between the horizontal acceleration $\bar{\ddot{u}}_s$ of the appurtenant secondary structure and the exciting frequency ω as

$$\bar{\ddot{u}}_s(\omega) = -\omega^2 \sum_{j=1}^{N_d+1} \tilde{\psi}_j^{(x)}(x_s, y_s)\, \bar{\tilde{Z}}_j(\omega) \tag{12}$$

where $\tilde{\psi}_j^{(x)}(x_s, y_s)$ denotes the x–component of the jth structural mode shape of the coupled system combining the dam and appurtenant secondary structure, taken along the SDOF representing the secondary structure, and $\bar{\tilde{Z}}_j$ is the corresponding generalized coordinate. The number of mode shapes included in the analysis is equal to that assuring convergence for the dam-reservoir system, i.e. N_d, plus one mode to account for the vibration of the secondary structure SDOF. The vector $\bar{\tilde{\mathbf{Z}}}$ of generalized coordinates $\bar{\tilde{Z}}_j$, $j = 1 \ldots N_d + 1$, can be obtained by solving the system of equations

$$\bar{\tilde{\mathbf{S}}}\, \bar{\tilde{\mathbf{Z}}} = \bar{\tilde{\mathbf{Q}}} \tag{13}$$

where, for $n = 1 \ldots N_d + 1$ and $j = 1 \ldots N_d + 1$

$$\bar{\tilde{S}}_{nj}(\omega) = \left[-\omega^2 + \left(1 + \mathrm{i}\,\eta_c \right) \tilde{\omega}_n^2 \right] \delta_{nj} + \omega^2 \int_0^{H_r} \bar{p}_j(0, y, \omega)\, \psi_n^{(x)}(0, y)\, \mathrm{d}y \tag{14}$$

$$\bar{\tilde{Q}}_n(\omega) = -\tilde{\psi}_n^{\mathrm{T}} \mathbf{M}_{cc}\, \mathbf{1} + \int_0^{H_r} \bar{p}_0(0, y, \omega)\, \psi_n^{(x)}(0, y)\, \mathrm{d}y \tag{15}$$

in which η_c, $\tilde{\omega}_n$, $\tilde{\psi}_n$ and $\mathbf{M}_{cc}$ are the hysteretic damping factor, natural frequency, structural mode shape and mass matrix corresponding to the coupled system combining the dam and secondary structure, respectively. We note that the integral terms in Eqs. (14) and (15) are the same as in Eqs. (8) and (9), respectively, since it is assumed that the presence of the dam-supported appurtenant structure does not affect hydrodynamic pressure within the reservoir.

To illustrate the application of the proposed FFRFs, the dynamic responses of two appurtenant secondary structures with fundamental frequencies of $5\,\mathrm{Hz}$ and $15\,\mathrm{Hz}$ are considered next. The secondary structures,

referred hereafter as the $5\,\text{Hz}$- and $15\,\text{Hz}$-systems, are attached to point A of coordinates (x_A, y_A) on the crest of each of dams D1 and D2 (Figs. 2 and 3). The coupled dam-secondary structure is assumed to have a hysteretic damping factor $\eta_\text{c} = 0.1$. Fig. 21 compares the FRFs $\bar{\bar{u}}_\text{A}$ of horizontal accelerations at point A, given by

$$\bar{\bar{u}}_\text{A}(\omega) = -\omega^2 \sum_{j=1}^{N_\text{d}} \psi_j^{(x)}(x_\text{A}, y_\text{A}) \, \bar{Z}_j(\omega) \tag{16}$$

to FFRFs $\bar{\bar{u}}_\text{s}$ of the secondary structures. The cases of (i) empty, (ii) compressible and (iii) incompressible water reservoirs are considered for comparison purposes. The peaks in the FRFs of Figs. 21 (a) and (b) correspond to the vibration frequencies of the dam-reservoir systems without the secondary structures. These FRFs also illustrate the effects of compressible or incompressible water assumptions with respect to the dynamic response of the empty dam. The FFRFs in Figs. 21 (c) to (f) first show that the relative differences between the amplitudes of the FFRFs corresponding to the three cases, i.e. empty, compressible and incompressible water reservoirs, depend on the exciting frequency as FRFs, but that they attenuate quickly after approximately $12\,\text{Hz}$ and $25\,\text{Hz}$ for the $5\,\text{Hz}$- and $15\,\text{Hz}$-systems, respectively. At dam D1, we observe that maximum acceleration response of the $5\,\text{Hz}$-system (respectively $15\,\text{Hz}$-system) is obtained when the dam impounds a compressible (resp. incompressible) water reservoir. At dam D2, maximum acceleration response of the $5\,\text{Hz}$-system (respectively $15\,\text{Hz}$-system) is obtained when the reservoir is empty (resp. full with an incompressible water assumption).

For all four cases, frequencies at which resonant responses occur include the fundamental frequencies of the dam-supported appurtenant structures. Comparison with the FRFs in Figs. 21 (a) and (b) reveals that the other resonant peaks correspond roughly to the frequencies of the dam alone or dam-reservoir systems, although slightly shifted in some cases due to interaction between the secondary structure and the rest of the system. For instance, for dam D1 with an empty reservoir, the first mode also corresponds to resonant responses of the dam with both secondary structures, while the effect of the second mode is attenuated for the dam supporting the $15\,\text{Hz}$-system, and considerably attenuated for the dam supporting the $5\,\text{Hz}$-system. The same applies to dam D1 impounding a compressible reservoir, except that the responses corresponding to the second and third modes of the dam-reservoir system are significantly flattened for both appurtenant secondary structures. When dam D1 impounds an incompressible reservoir, the resonant response corresponding to the first mode of the dam-reservoir system is slightly shifted towards lower frequencies for both secondary systems, as well as the attenuated response corresponding to the second mode for the $15\,\text{Hz}$-system. For higher dam D2, practically the same previous analysis can be applied, except that the frequency shifts are less pronounced than for dam D1. We also observe a larger amplification of accelerations at the fundamental frequencies of $5\,\text{Hz}$ and $15\,\text{Hz}$ of the secondary structures since these frequencies are close to those corresponding to the fundamental mode for the empty dam and third mode of the dam impounding an incompressible reservoir.

4 Conclusions

This paper presented an original investigation of the sensitivity of floor acceleration demands in gravity dams to various modeling assumptions of the impounded reservoir. Two techniques were used to obtain floor acceleration demands: a coupled dam-reservoir finite element model and a semi-infinite reservoir analytical model. Both techniques were applied to typical dam-reservoir systems with different geometries. The dam-reservoir systems were subjected to ground motions with various frequency contents and the resulting floor acceleration demands within the dams were studied through examination of floor acceleration spectra obtained at the crest of the studied dams, and maximum floor acceleration demands along their height. A detailed analysis of the effects of reservoir geometry, water compressibility, reservoir bottom wave absorption and dam higher vibration modes was presented. Seismic demands within the dams with empty reservoirs were also determined for comparison purposes. The following main conclusions could be drawn:

– If the geometry of the reservoir is assumed rectangular, a truncation length equal to four times the height of the reservoir was found to be a good compromise between accuracy and efficient numerical computation of floor acceleration demands within the studied dams subjected to the ground motions considered.

– Fluid-structure interaction effects are generally significant in the evaluation of floor acceleration demands, except at the very low frequency range. It was found that these effects can lead to amplification or reduction of floor acceleration demands with respect to the empty reservoir case.

– Reservoir geometry cannot always be assumed rectangular as usually done in practical 2D seismic analyses, as higher floor acceleration demands can be induced by irregular reservoir geometries as illustrated by the case studies in the paper. Reservoir geometry effects were found to attenuate with increasing energy dissipation due to higher reservoir bottom wave absorption. These effects also vanish if water in the reservoir is assumed incompressible.

– The dynamic response of a dam-supported appurtenant structure can be affected by energy dissipation at reservoir bottom according to trends corresponding to increasing or decreasing floor acceleration demands with lower reservoir bottom wave absorption. Maximum effects are however generally concentrated around the main resonant segments of the floor acceleration spectra.

– The results revealed a high sensitivity of floor acceleration demands to reservoir modeling assumptions as added masses, incompressible or compressible water domain. Water compressibility was found to affect the dynamic response of dam-supported appurtenant structures differently depending on the dam and frequency ranges considered. Floor acceleration demands corresponding to the three assumptions are however practically identical in the low frequency range.

– Fundamental mode analysis can be sufficient to obtain low frequency range floor acceleration demands within rigid dams, while more modes are required to assess the dynamic response of appurtenant secondary structures vibrating at larger frequencies on more flexible dams.

Finally, floor frequency response functions were developed to assess floor acceleration demands at the

stage of preliminary seismic design or safety evaluation of dam-supported appurtenant structures. We showed through examples that the proposed approach can be effectively used to compare floor acceleration demands within different dams or within the same dam considering various modeling assumptions of the reservoir.

Acknowledgements

References

ADINA Theory and Modeling Guide. Report ARD 06-7. ADINA R & D Inc.; 2011.

Arcangeli E, Ciabarri P. Menjil dam rehabilitation by resin grouting and high capacity anchors. Water Power Dam Construct 1994; 46:19–25.

Asfura A, Der Kiureghian A. Floor Response Spectrum Method for Seismic Analysis of Multiply Supported Secondary Systems. Earthquake Engineering and Structural Dynamics 1986;14:245-65.

Ben Ftima M, Léger P. Seismic stability of cracked concrete dams using rigid block models Computers and Structures 2006;84:1802–1814.

Boore DM, Atkinson GM. Source spectra for the 1988 Saguenay, Québec, Earthquakes. Bulletin of the Seismological Society of America 1992;82:683-719.

Bouaanani N, Lu FY. Assessment of potential-based fluid finite elements for seismic analysis of dam–reservoir systems. Journal of Computers and Structures 2009;87:206-24.

Bouaanani N, Goulmot D, Miquel B. Seismic response of asymmetric rectangular liquid containing structures. ASCE Journal of Engineering Mechanics 2012;138:1288-1297.

Chen Y, Soong T-T. Seismic response of secondary systems. Engineering Structures 1988;10:218-28.

Chopra AK. Earthquake response of concrete gravity dams. University of California, Berkeley: Report UCB/EERC-70/01; 1970.

Donlon WP, Hall JF. Shake table study of concrete dam monoliths. Earthq Eng Struct Dynam 1991;20:769-86.

Everstine GC. A symmetric potential formulation for fluid-structure interaction. Journal of Sound and Vibration 1981;79(1):157-60.

Fenves G, Chopra AK. Earthquake analysis and response of concrete gravity dams. University of California, Berkeley: Report UCB/EERC-84/10; 1984.

GSC, Earthquakes Canada, Geological Survey of Canada, http://earthquakescanada.nrcan.gc.ca, Date accessed: 27 September 2006.

Hall JF, Chopra AK. Two-dimensional dynamic analysis of concrete gravity and embankment dams including hydrodynamic effects. Earthquake Engineering and Structural Dynamics 1982;10:305-32.

Hamdan FH, Dowling PJ. Far-field fluid-structure interaction—Formulation and validation. Computers and Structures 1995;56(6):949-58.

Humar JL, Jablonski AM. Boundary element reservoir model for seismic analysis of gravity dams. Earthquake Engineering and Structural Dynamics 1988;16:1129-56.

Hansen KD, Roehm LH. The response of concrete dams to earthquakes. Water Power Dam Construct 1979;31(4):27–31.

International Commission on Large Dams (ICOLD). Design features of dams to resist seismic ground motion, guidelines and case studies, Bulletin 120; 2001.

International Commission on Large Dams (ICOLD). Selecting seismic parameters for large dams, Bulletin 72; 2010.

Lin G, Zhou J, Fan C. Dynamic model rupture test and safety evaluation of concrete gravity dams. Dam Eng, 1993;4(3):173–86.

Lysmer J, Kuhlemeyer RL. Finite dynamic model for infinite media. Journal of the Engineering Mechanics Division ASCE 1969;95:859-77.

Malla S, Wieland M. Simple model for safety assessment of cracked concrete dams subjected to strong ground shaking. Proceedings International Commission on Large Dams, 21st Congress, vol. Q83-R11. Montréal, Canada; 2003. p. 151--67.

Matsumoto N, Sasaki T, Ohmachi T. The 2011 Tohoku Earthquake and Dams, Proceedings of 79th ICOLD Annual Meeting, June 2011, Lucerne, Switzerland; 2011.

Olson LG, Bathe KJ. Analysis of fluid-structure interactions: a direct symmetric coupled formulation based on the fluid velocity potential. Computers and Structures 1985;21(1):21-32.

Olson LG, Bathe KJ. An infinite element for analysis of transient fluid—structure interactions. Engineering Computations 1985;2(4):319-29.

Pacific Earthquake Engineering Research Center (PEER) - Strong Motion Database, http://peer.berkeley.edu/smcat/, Date accessed: 15 September 2012.

Rainer JH, Dascal O. Behaviour of instrumented Hydro-Québec Dams during the Saguenay Earthquake. Proceedings of Canadian Dam Safety Conference, 16 September, Whistler, BC, Canada; 1991. p. 189-202.

Singh MP. Generation of seismic floor spectra. Journal of Engineering Mechanics Division ASCE 1975;101:593-607.

Singh MP. Seismic design input for secondary system. Journal of Engineering Mechanics Division ASCE 1980;106:505-617.

Singh MP. Seismic Floor Spectra by Mode Acceleration Approach. Journal Engineering Mechanics Division ASCE 1985;111:1402-19.

Sommerfeld A. Partial differential equations in physics. Academic Press, New York; 1949.

Tinawi R, Léger P, Leclerc M, Cipolla G. Seismic safety of gravity dams: From shake table experiments to numerical analyses. J. Struct. Eng. 2000;126(4):518-29.

United States Committee on Large Dams (USCOLD). Observed Performance of Dam During Earthquakes, Volume II, Denver; 2000.

Wei K, Yuan W, Bouaanani N. Experimental and numerical assessment of the three-dimensional modal dynamic response of bridge pile foundations submerged in water. ASCE Journal of Bridge Engineering 2013;18:1032–1041.

Westergaard HM. Water pressure on dams during earthquakes. Transactions ASCE 1933;98:418-72.

Wieland M, Malla S. Earthquake safety of an arch-gravity dam with a horizontal crack in the upper portion of the dam. Proceedings of the 12th World Conference on Earthquake Engineering, paper no. 1779, Auckland, New Zealand; 2000.

Zienkiewicz OC, Newton RE. Coupled vibrations in a structure submerged in a compressible fluid. International Symposium on Finite Element Techniques, Stuttgart; 1969.

List of figures

mands at the crest of dam D2 subjected to: (a) and (b) Imperial Valley (1940) ground motion; (c) and (d) Parkfield (1966) ground motion; (e) and (f) Loma Prieta (1989) ground motion; and (g) and (h) Saguenay (1988) ground motion.

Fig. 11: Effects of reservoir bottom wave absorption and reservoir geometry of the maximum floor acceleration demands along the height of dam D1 subjected to: (a) and (b) Imperial Valley (1940) ground motion; (c) and (d) Parkfield (1966) ground motion; (e) and (f) Loma Prieta (1989) ground motion; and (g) and (h) Saguenay (1988) ground motion.

Fig. 12: Effects of reservoir bottom wave absorption and reservoir geometry of the maximum floor acceleration demands along the height of dam D2 subjected to: (a) and (b) Imperial Valley (1940) ground motion; (c) and (d) Parkfield (1966) ground motion; (e) and (f) Loma Prieta (1989) ground motion; and (g) and (h) Saguenay (1988) ground motion.

Fig. 13: Effects of water modeling assumptions on floor acceleration demands at the crest of dam D1 subjected to: (a) and (b) Imperial Valley (1940) ground motion; (c) and (d) Parkfield (1966) ground motion; (e) and (f) Loma Prieta (1989) ground motion; and (g) and (h) Saguenay (1988) ground motion.

Fig. 14: Effects of water modeling assumption on the floor acceleration demands at the crest of dam D2 subjected to: (a) and (b) Imperial Valley (1940) ground motion; (c) and (d) Parkfield (1966) ground motion; (e) and (f) Loma Prieta (1989) ground motion; and (g) and (h) Saguenay (1988) ground motion.

Fig. 15: Effects of water modeling assumption on maximum floor acceleration demands along the height of dam D1 subjected to: (a) and (b) Imperial Valley (1940) ground motion; (c) and (d) Parkfield (1966) ground motion; (e) and (f) Loma Prieta (1989) ground motion; and (g) and (h) Saguenay (1988) ground motion.

Fig. 16: Effects of water modeling assumption on maximum floor acceleration demands along the height of dam D2 subjected to: (a) and (b) Imperial Valley (1940) ground motion; (c) and (d) Parkfield (1966) ground motion; (e) and (f) Loma Prieta (1989) ground motion; and (g) and (h) Saguenay (1988) ground motion.

Fig. 17: Effect of the number of structural modes included in the analysis on floor acceleration demands at the crest of dam D1 subjected to: (a) and (b) Imperial Valley (1940) ground motion; (c) and (d) Parkfield (1966) ground motion; (e) and (f) Loma Prieta (1989) ground motion; and (g) and (h) Saguenay (1988) ground motion.

Fig. 18: Effect of the number of structural modes included in the analysis on maximum floor acceleration demands along the height of dam D1 subjected to: (a) and (b) Imperial Valley (1940) ground motion; (c) and (d) Parkfield (1966) ground motion; (e) and (f) Loma Prieta (1989) ground motion;

and (g) and (h) Saguenay (1988) ground motion.

Fig. 19: Effect of the number of structural modes included in the analysis on floor acceleration demands at the crest of dam D2 subjected to: (a) and (b) Imperial Valley (1940) ground motion; (c) and (d) Parkfield (1966) ground motion; (e) and (f) Loma Prieta (1989) ground motion; and (g) and (h) Saguenay (1988) ground motion.

Fig. 20: Effect of the number of structural modes included in the analysis on maximum floor acceleration demands along the height of dam D2 subjected to: (a) and (b) Imperial Valley (1940) ground motion; (c) and (d) Parkfield (1966) ground motion; (e) and (f) Loma Prieta (1989) ground motion; and (g) and (h) Saguenay (1988) ground motion.

Fig. 21: FRFs and FFRFs of the horizontal accelerations considering empty, compressible and incompressible water reservoirs: (a) FRF for dam D1; (b) FRF for dam D2; (c) FFRF for 5 Hz-system at the crest of dam D1; (d) FFRF for 5 Hz-system at the crest of dam D2; (e) FFRF for 15 Hz-system at the crest of dam D1; (f) FFRF for 15 Hz-system at the crest of dam D2.
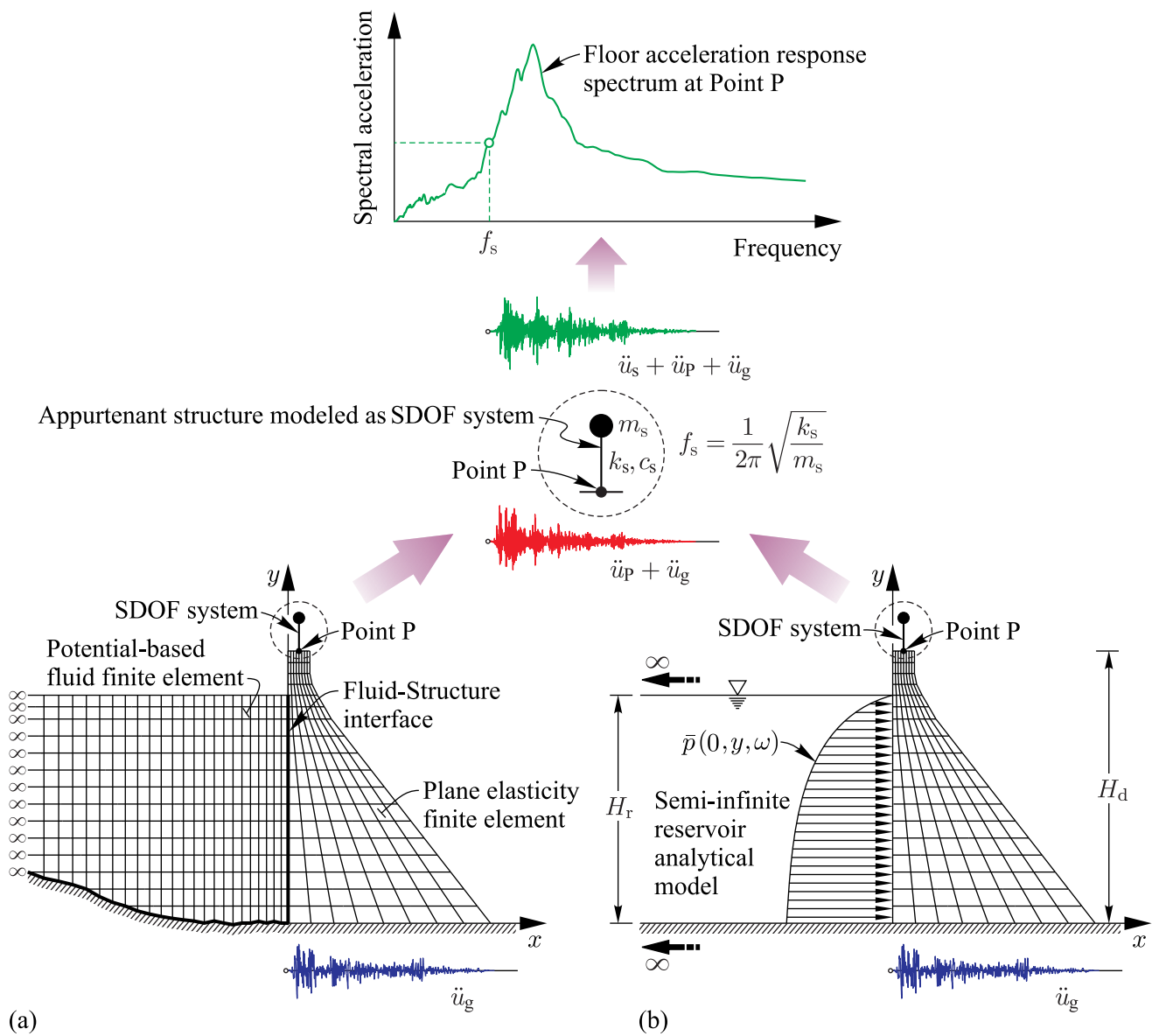
Figure 1. Illustration of the computation of floor acceleration spectra at a given point P of a gravity dam: (a) using a coupled dam-reservoir finite element model; and (b) using a semi-infinite reservoir analytical model.

(a)

$L_r = 128.0$ m
5.0 m
Infinite fluid elements
Free surface boundary condition
32.0 m
Point A
Point B
30.0 m
$H_d = 35.0$ m
0.0 m
Earthquake excited boundary
3-node beam element e
Potential-based fluid element
Point C
27.5 m

Viscous dampers $\begin{cases} c_1^{(e)} = \dfrac{1}{6}\Lambda\ell^{(e)} & c_2^{(e)} = \dfrac{1}{6}\Lambda\ell^{(e)} \\ c_3^{(e)} = \dfrac{2}{3}\Lambda\ell^{(e)} & \Lambda = \rho_r C_r\left(\dfrac{1+\alpha}{1-\alpha}\right) \end{cases}$

$\ell^{(e)}$

(b)

$L_r = 128.0$ m
5.0 m
Infinite fluid elements
Free surface boundary condition
32.0 m
Point A
Point B
30.0 m
$H_d = 35.0$ m
0.0 m
4.0°
Earthquake excited boundary
22.4°
Viscous dampers
11.4°
4.5°
Point C

49.9 m
23.5 m
28.6 m
26.0 m
27.5 m

Figure 2. Dimensions of the 35 m-high dam (D1) impounding reservoirs with: (a) rectangular, (b) and irregular geometries.

(a)

$L_r = 344.0$ m — 5.0 m

Infinite fluid elements

Free surface boundary condition

86.0 m

Point A
Point B

82.0 m

$H_d = 90.0$ m

0.0 m

Earthquake excited boundary

Point C

70.0 m

3-node beam element e

Potential-based fluid element

Viscous dampers $\begin{cases} c_1^{(e)} = \dfrac{1}{6}\Lambda\ell^{(e)} & c_2^{(e)} = \dfrac{1}{6}\Lambda\ell^{(e)} \\ c_3^{(e)} = \dfrac{2}{3}\Lambda\ell^{(e)} & \Lambda = \rho_r C_r\left(\dfrac{1+\alpha}{1-\alpha}\right) \end{cases}$

$\ell^{(e)}$

(b)

$L_r = 344.0$ m — 5.0 m

Infinite fluid elements

Free surface boundary condition

86.0 m

Point A
Point B

82.0 m

$H_d = 90.0$ m

0.0 m

4.0°

Earthquake excited boundary

22.4°

Viscous dampers

11.4°

4.5°

Point C

134.0 m — 63.0 m — 77.0 m — 70.0 m — 70.0 m

Figure 3. Dimensions of the 90 m-high dam (D2) impounding reservoirs with: (a) rectangular, (b) and irregular geometries.
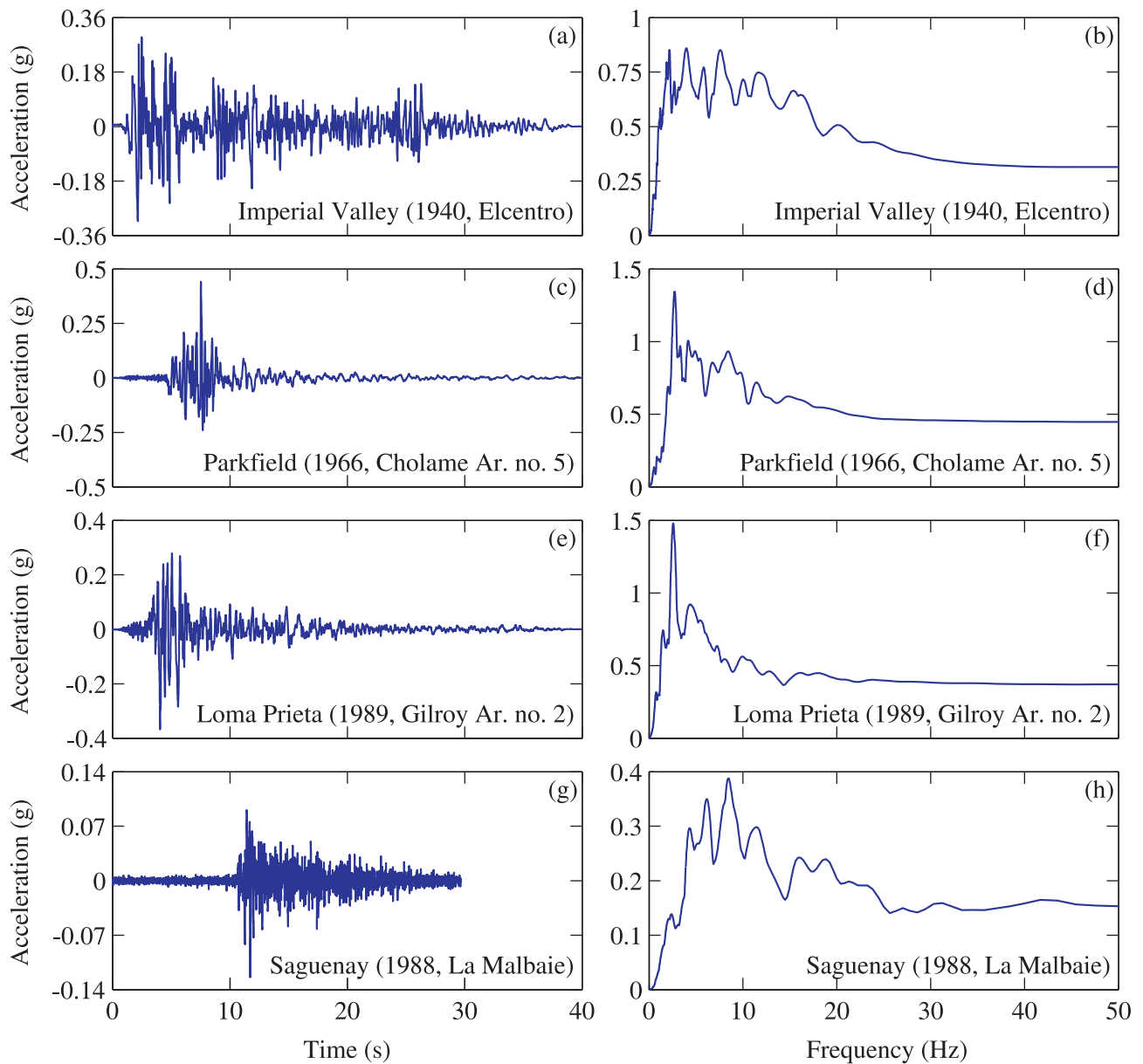
Figure 4. Acceleration time-histories and 5%-damped acceleration spectra of the ground motions considered: (a) and (b) Imperial Valley earthquake (1940) horizontal component at Elcentro ; (c) and (d) Parkfield earthquake (1966) horizontal component at Cholame Array no. 5 ; (e) and (f) Loma Prieta earthquake (1989) horizontal component at Gilroy Array no. 2 ; (g) and (h) Saguenay earthquake (1988) horizontal component at La Malbaie. (a), (c), (e) and (g): Acceleration time-histories; (b), (d), (f) and (h): Acceleration spectra.
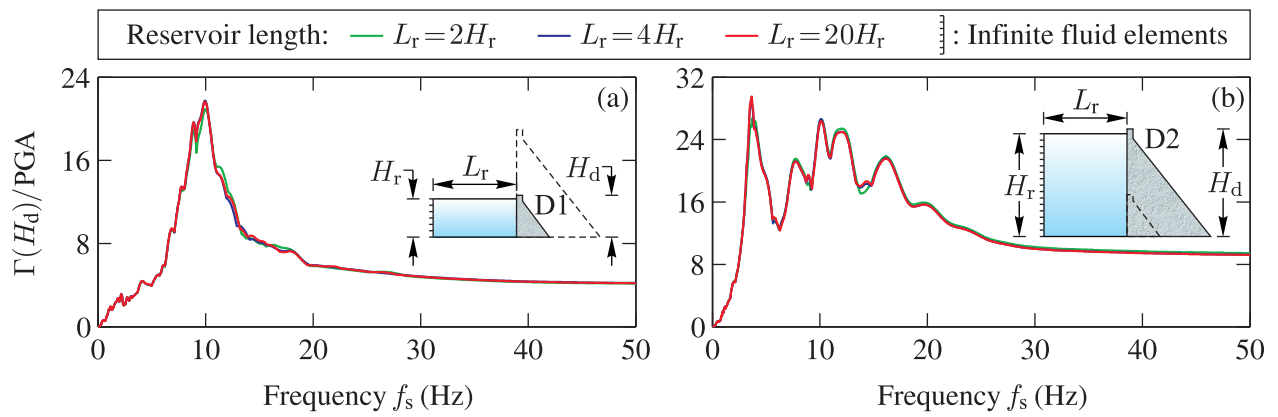
Figure 5. Floor acceleration demands at the crests of dams D1 and D2 subjected to Imperial Valley earthquake considering truncation lengths $L_r = 2H_r$, $L_r = 4H_r$ and $L_r = 20H_r$: (a) Dam D1, and (b) Dam D2.
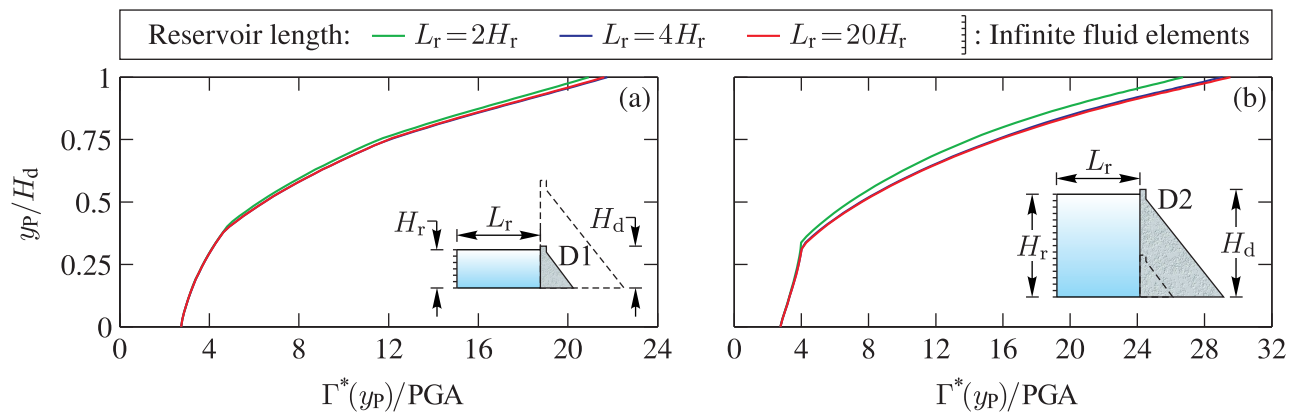
Figure 6. Peak floor acceleration demands along the height of dams D1 and D2 subjected to Imperial Valley earthquake considering truncation lengths $L_r = 2H_r$, $L_r = 4H_r$ and $L_r = 20H_r$: (a) Dam D1, and (b) Dam D2.
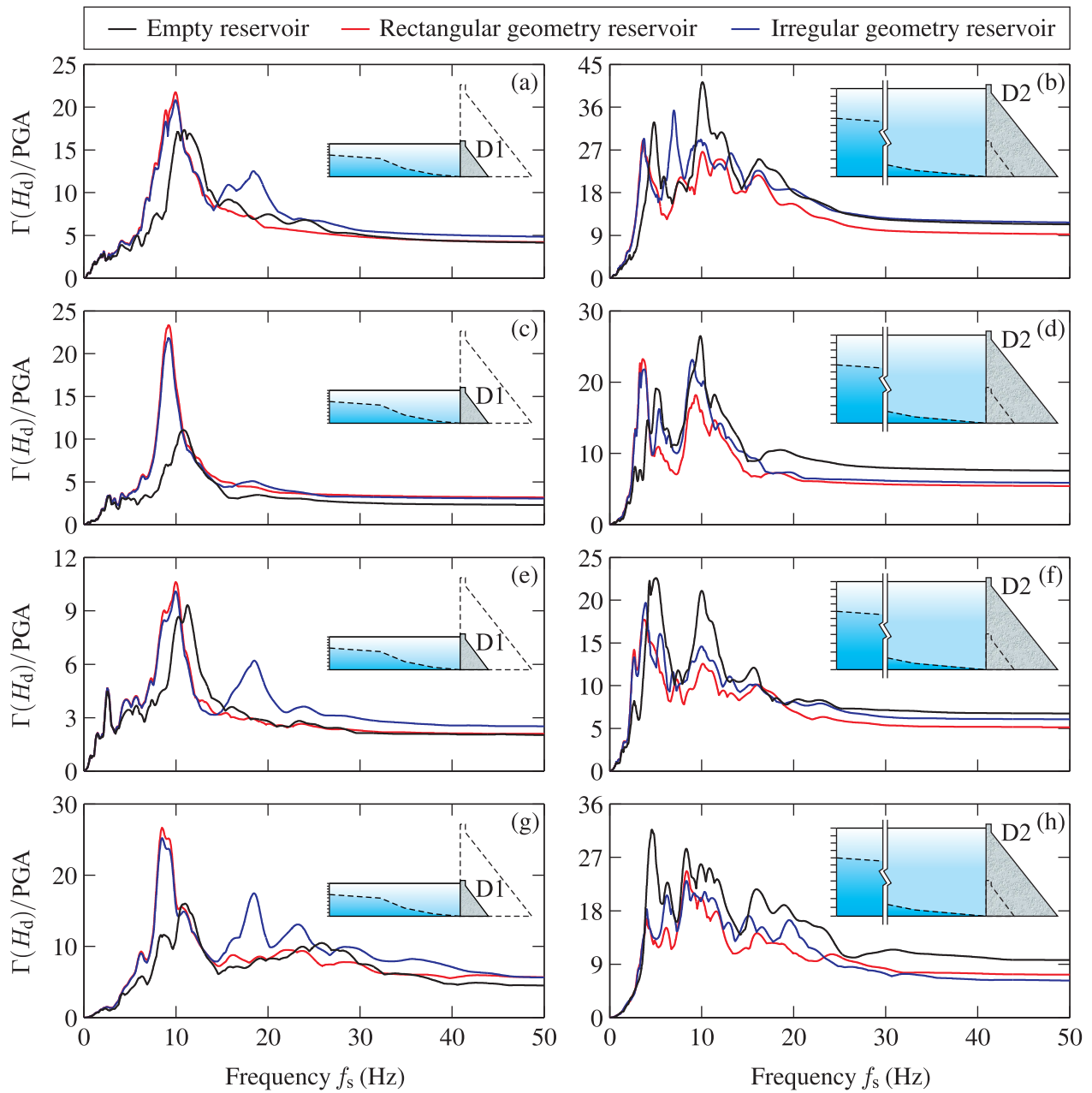
Figure 7. Floor acceleration demands at the crests of dams D1 and D2 impounding rectangular and irregular geometry reservoirs and subjected to: (a) and (b) Imperial Valley (1940) ground motion; (c) and (d) Parkfield (1966) ground motion; (e) and (f) Loma Prieta (1989) ground motion; and (g) and (h) Saguenay (1988) ground motion.
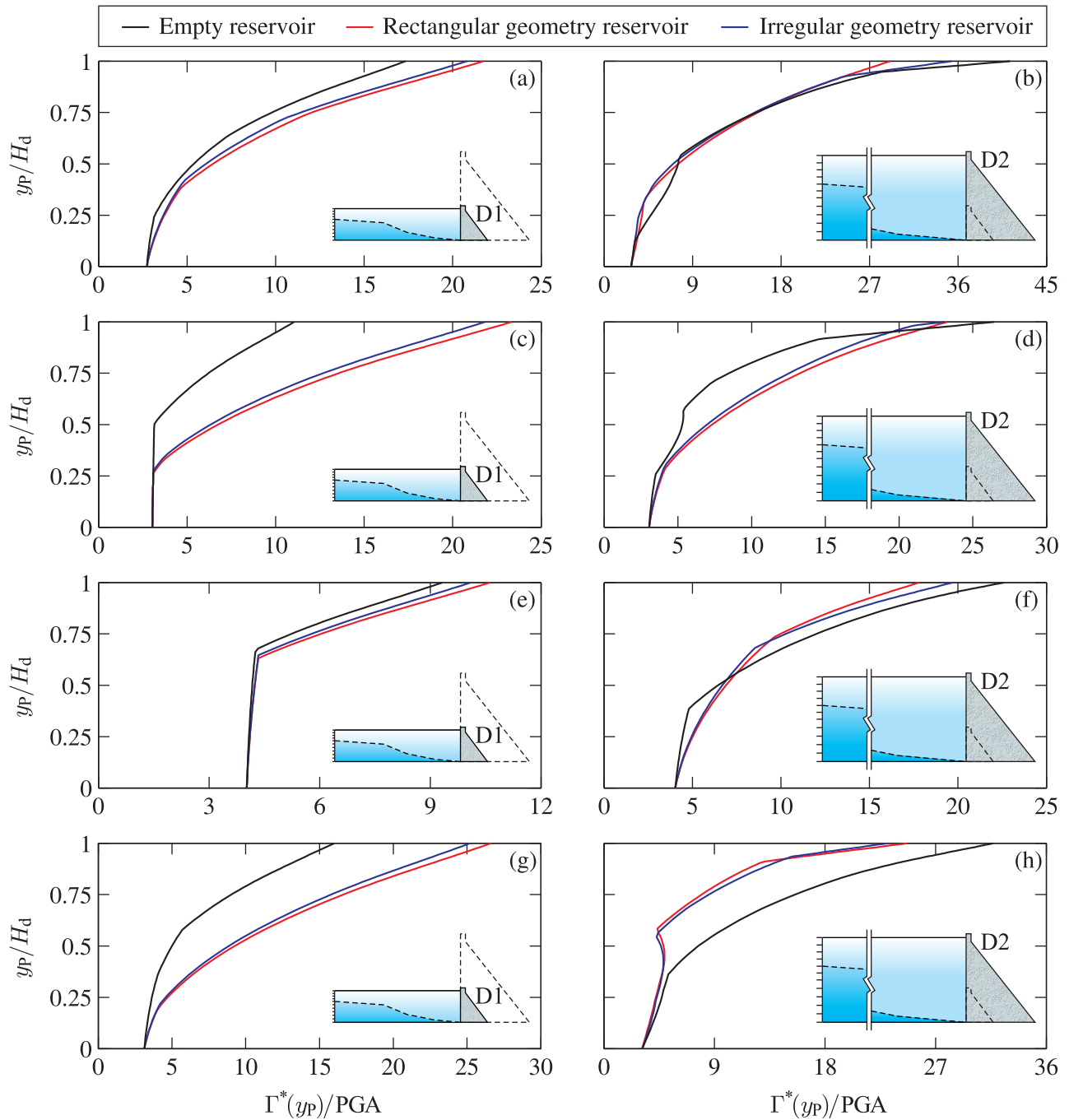
Figure 8. Maximum floor acceleration demands along the height of dams D1 and D2 impounding rectangular and irregular geometry reservoirs and subjected to: (a) and (b) Imperial Valley (1940) ground motion; (c) and (d) Parkfield (1966) ground motion; (e) and (f) Loma Prieta (1989) ground motion; and (g) and (h) Saguenay (1988) ground motion.
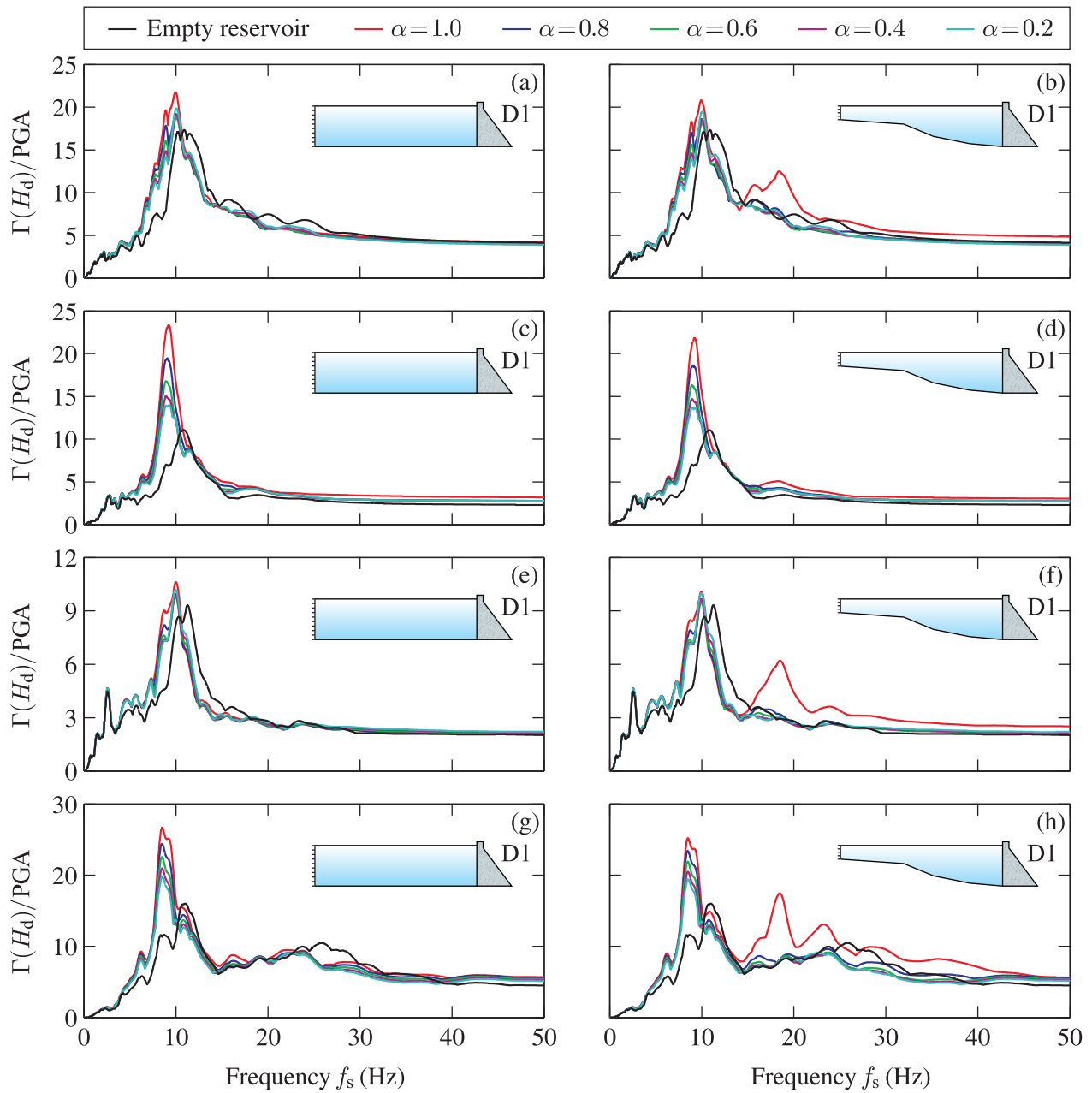
Figure 9. Effects of reservoir bottom wave absorption and reservoir geometry of the floor acceleration demands at the crest of dam D1 subjected to: (a) and (b) Imperial Valley (1940) ground motion; (c) and (d) Parkfield (1966) ground motion; (e) and (f) Loma Prieta (1989) ground motion; and (g) and (h) Saguenay (1988) ground motion.
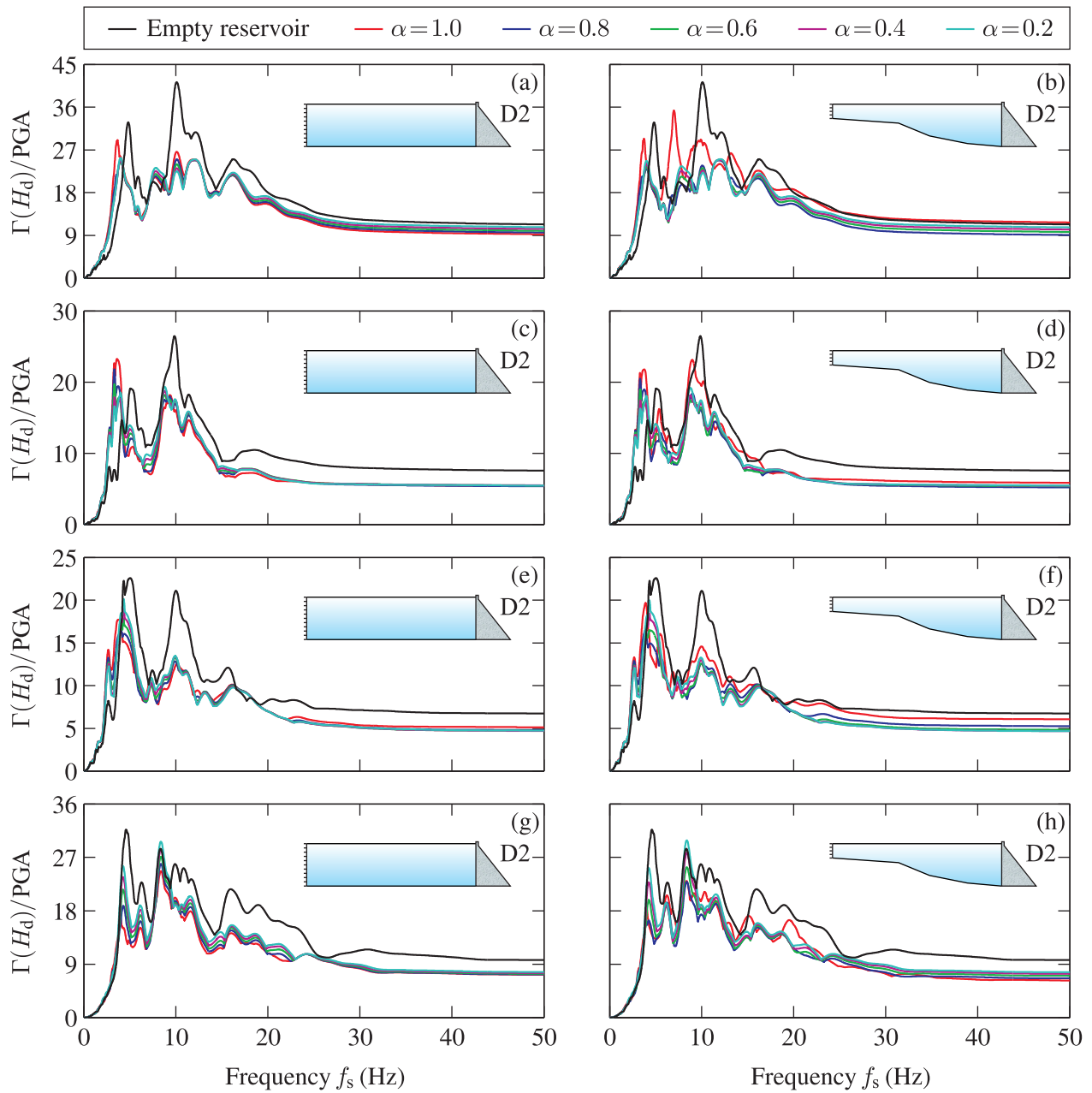
Figure 10. Effects of reservoir bottom wave absorption and reservoir geometry of the floor acceleration demands at the crest of dam D2 subjected to: (a) and (b) Imperial Valley (1940) ground motion; (c) and (d) Parkfield (1966) ground motion; (e) and (f) Loma Prieta (1989) ground motion; and (g) and (h) Saguenay (1988) ground motion.
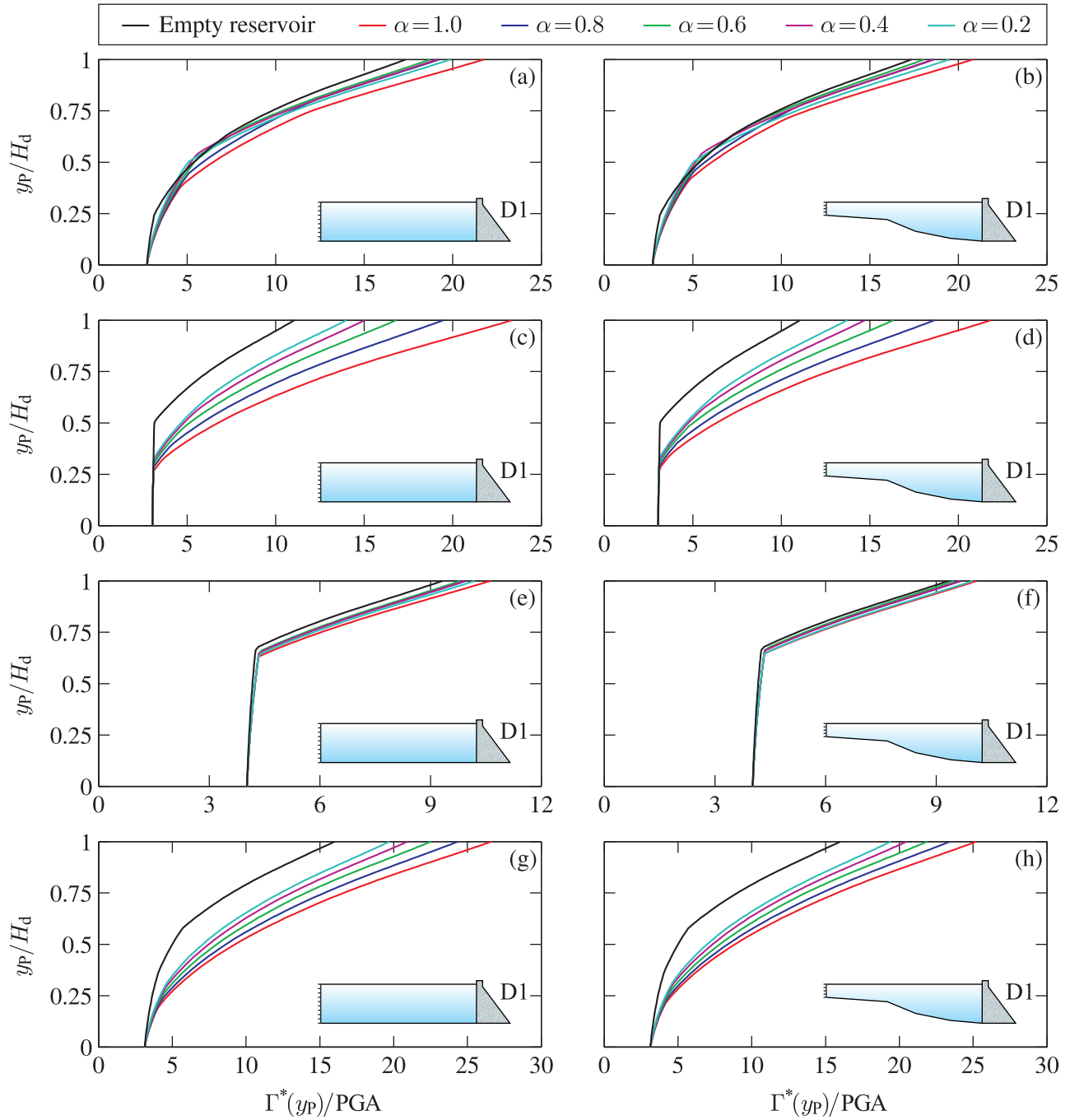
Figure 11. Effects of reservoir bottom wave absorption and reservoir geometry of the maximum floor acceleration demands along the height of dam D1 subjected to: (a) and (b) Imperial Valley (1940) ground motion; (c) and (d) Parkfield (1966) ground motion; (e) and (f) Loma Prieta (1989) ground motion; and (g) and (h) Saguenay (1988) ground motion.
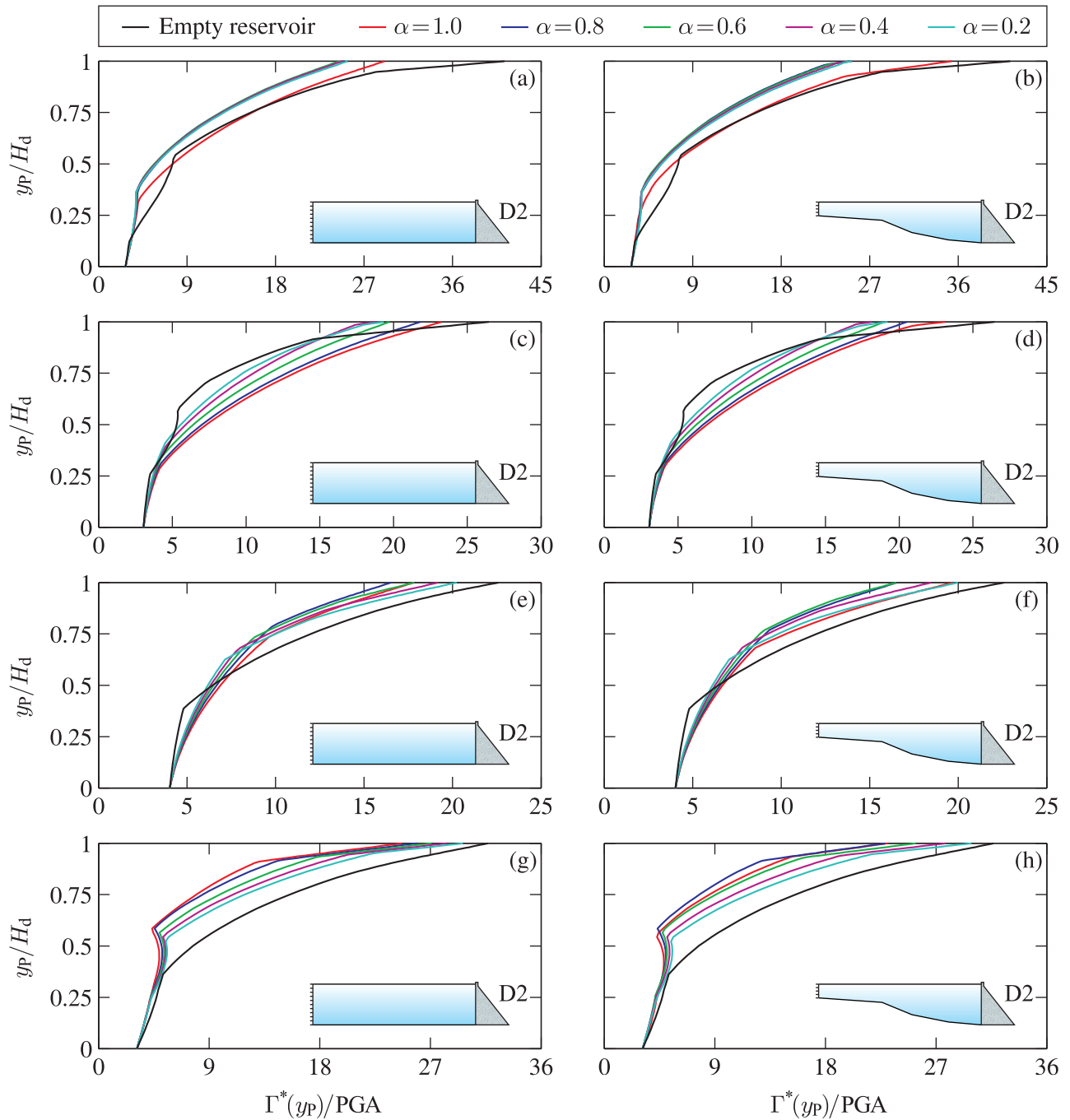
Figure 12. Effects of reservoir bottom wave absorption and reservoir geometry of the maximum floor acceleration demands along the height of dam D2 subjected to: (a) and (b) Imperial Valley (1940) ground motion; (c) and (d) Parkfield (1966) ground motion; (e) and (f) Loma Prieta (1989) ground motion; and (g) and (h) Saguenay (1988) ground motion.
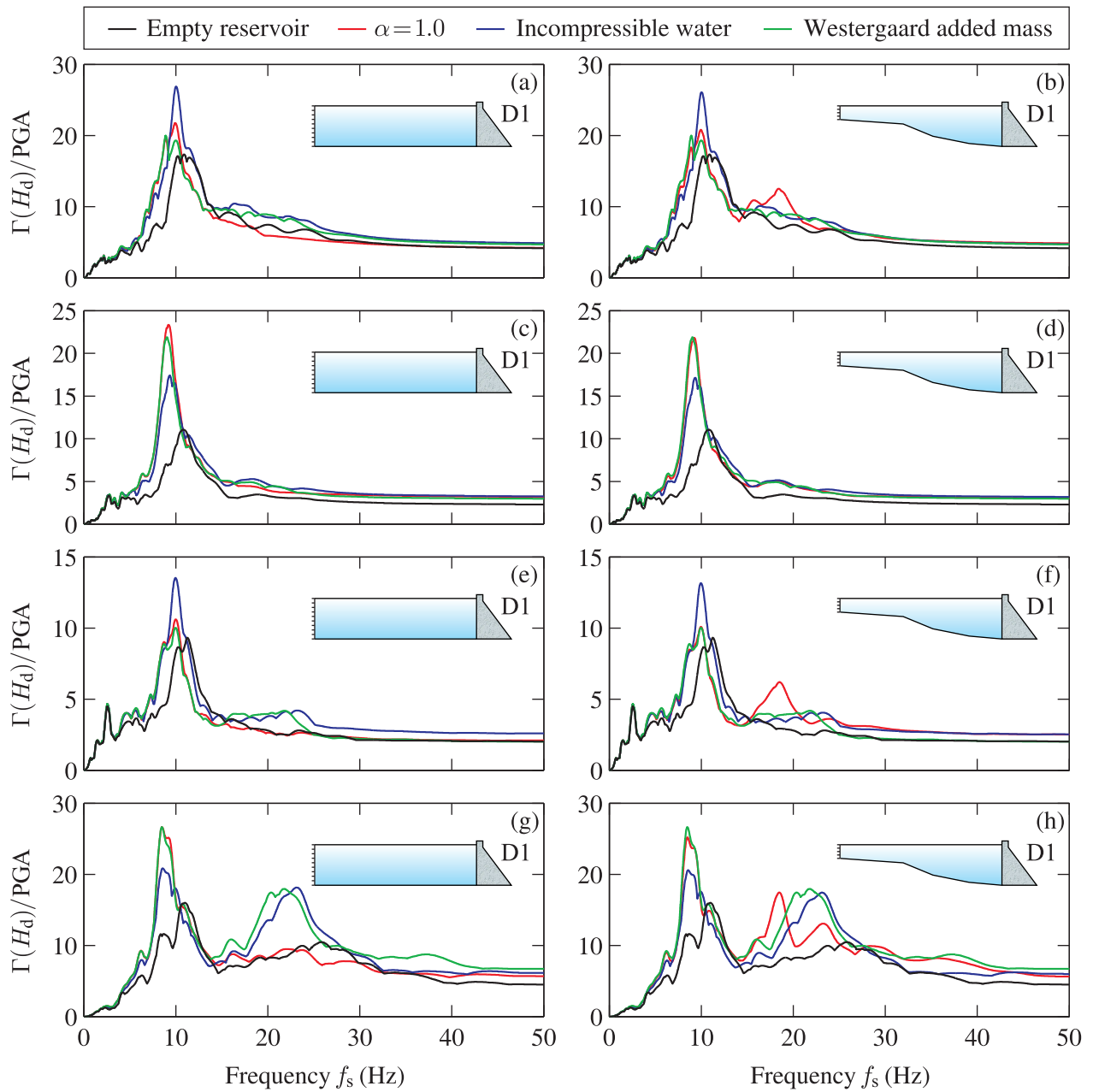
Figure 13. Effects of water modeling assumptions on floor acceleration demands at the crest of dam D1 subjected to: (a) and (b) Imperial Valley (1940) ground motion; (c) and (d) Parkfield (1966) ground motion; (e) and (f) Loma Prieta (1989) ground motion; and (g) and (h) Saguenay (1988) ground motion.
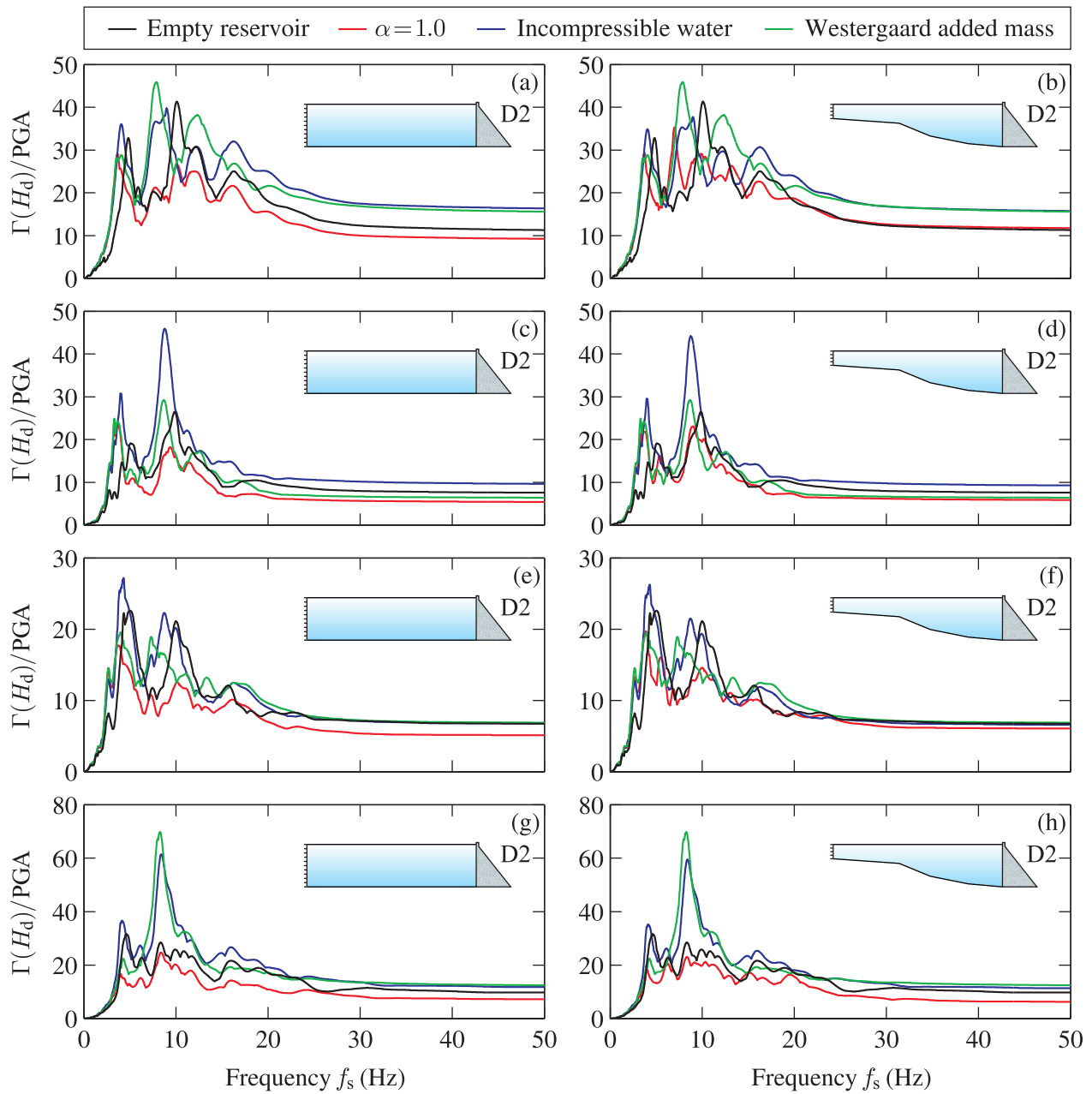
Figure 14. Effects of water modeling assumption on the floor acceleration demands at the crest of dam D2 subjected to: (a) and (b) Imperial Valley (1940) ground motion; (c) and (d) Parkfield (1966) ground motion; (e) and (f) Loma Prieta (1989) ground motion; and (g) and (h) Saguenay (1988) ground motion.
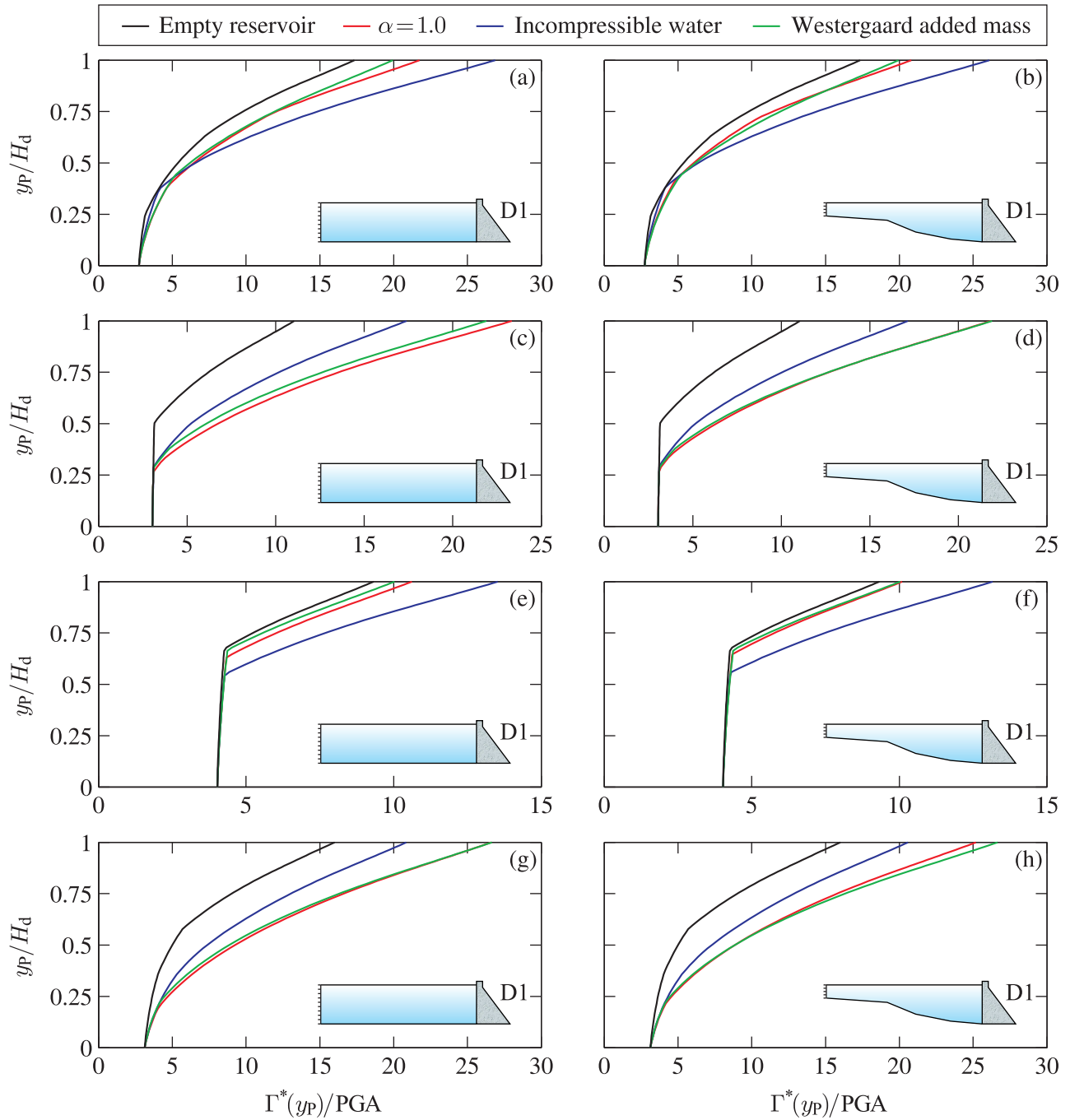
Figure 15. Effects of water modeling assumption on maximum floor acceleration demands along the height of dam D1 subjected to: (a) and (b) Imperial Valley (1940) ground motion; (c) and (d) Parkfield (1966) ground motion; (e) and (f) Loma Prieta (1989) ground motion; and (g) and (h) Saguenay (1988) ground motion.
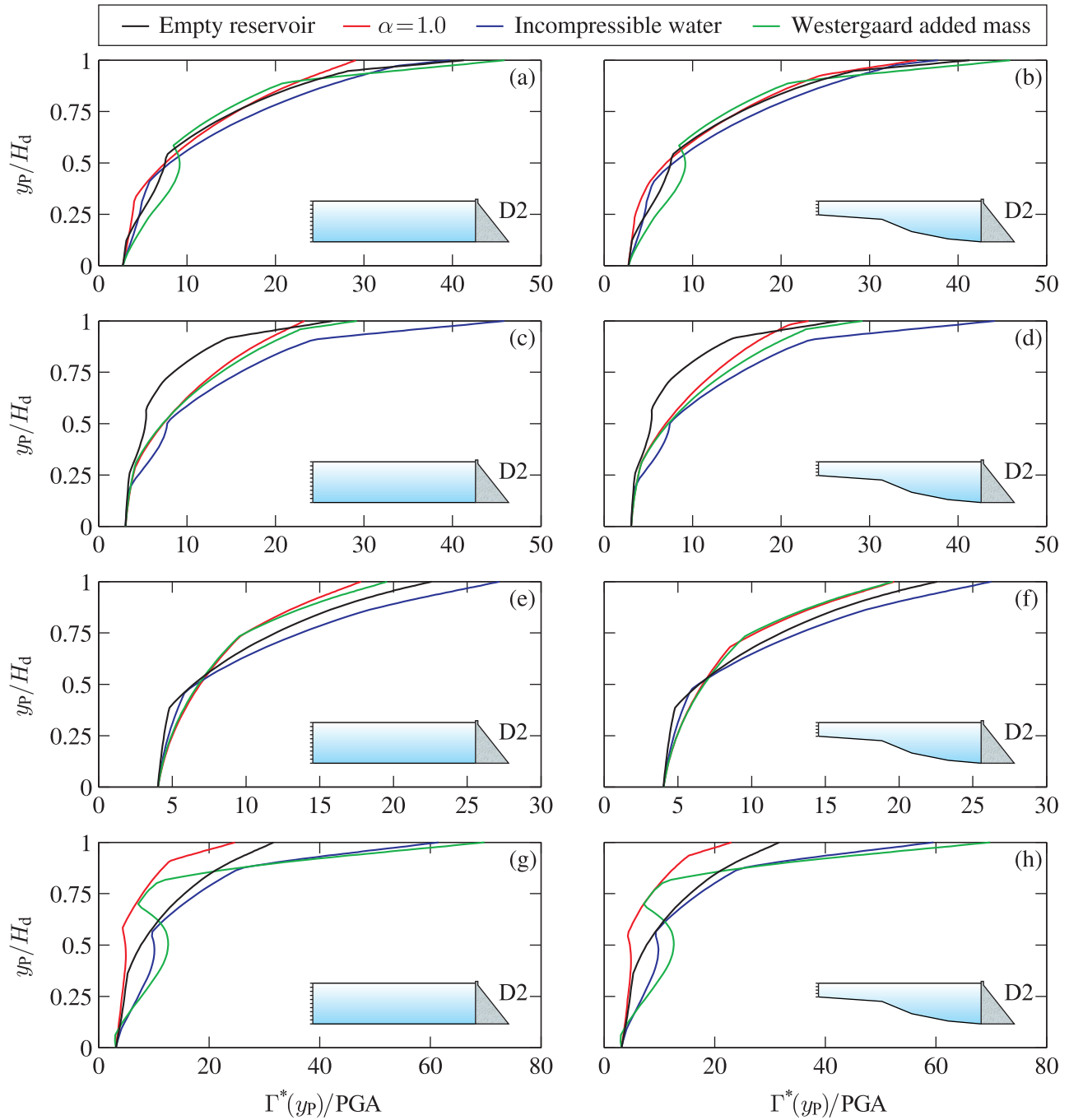
Figure 16. Effects of water modeling assumption on maximum floor acceleration demands along the height of dam D2 subjected to: (a) and (b) Imperial Valley (1940) ground motion; (c) and (d) Parkfield (1966) ground motion; (e) and (f) Loma Prieta (1989) ground motion; and (g) and (h) Saguenay (1988) ground motion.
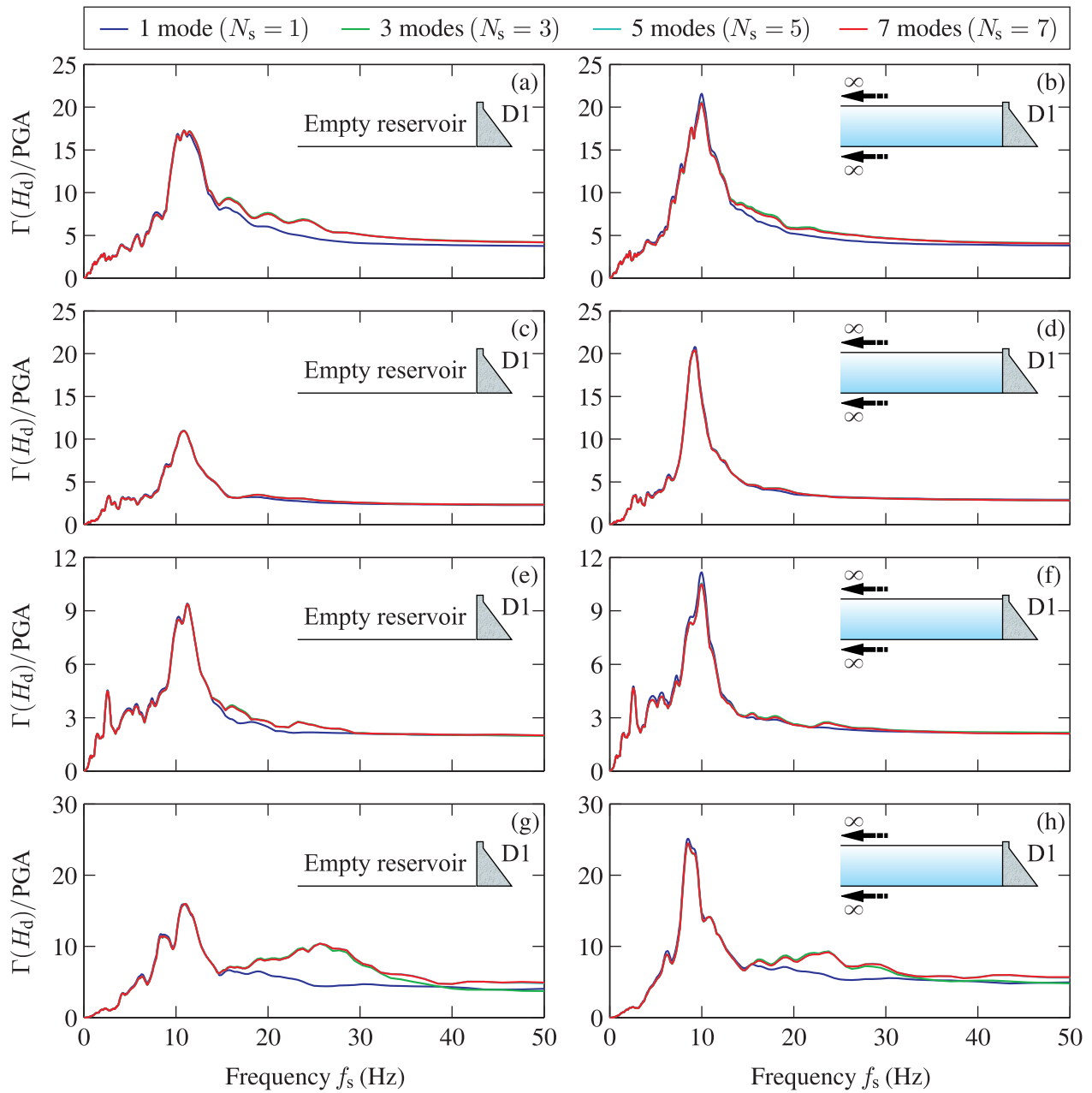
Figure 17. Effect of the number of structural modes included in the analysis on floor acceleration demands at the crest of dam D1 subjected to: (a) and (b) Imperial Valley (1940) ground motion; (c) and (d) Parkfield (1966) ground motion; (e) and (f) Loma Prieta (1989) ground motion; and (g) and (h) Saguenay (1988) ground motion.
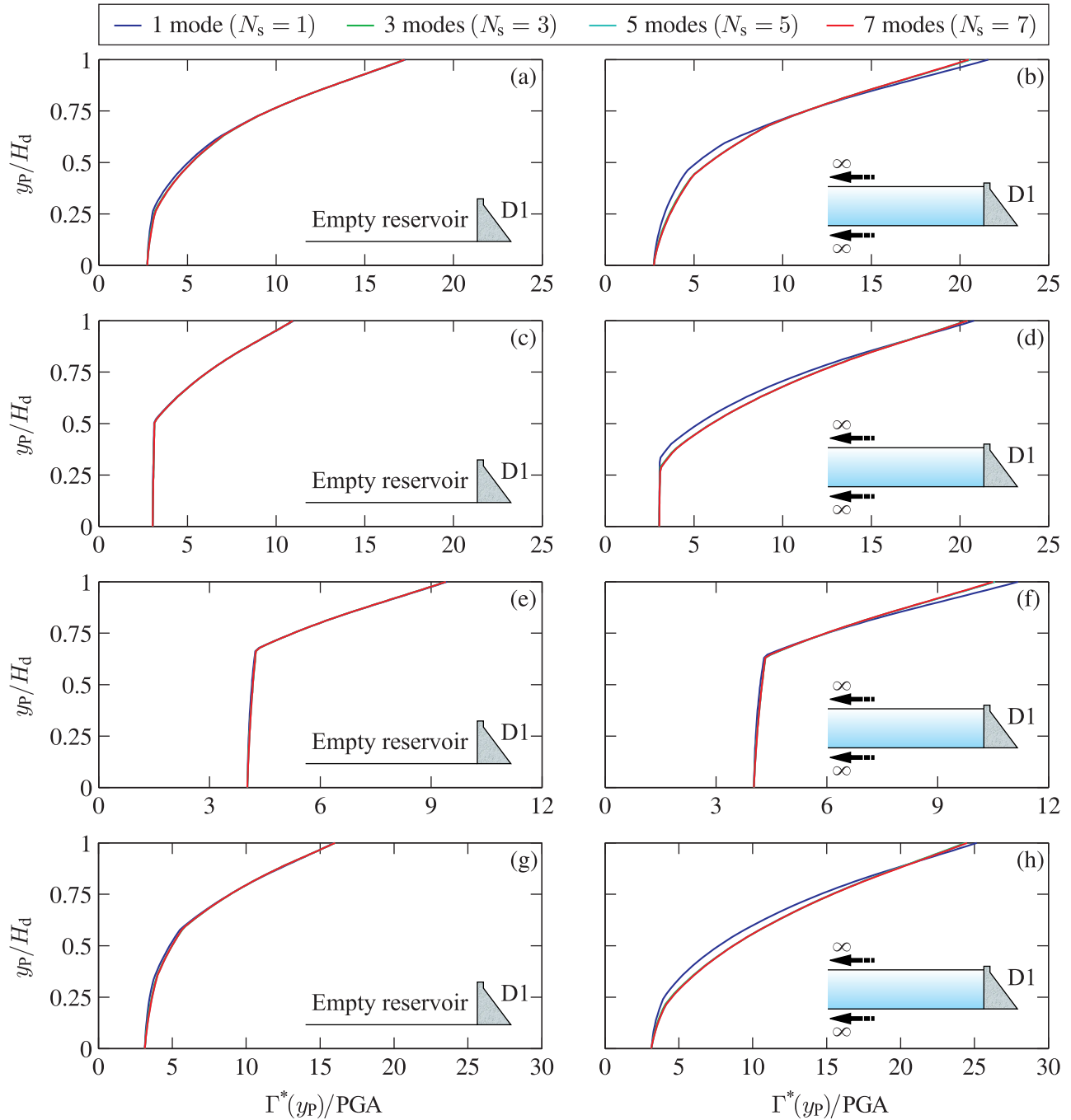
Figure 18. Effect of the number of structural modes included in the analysis on maximum floor acceleration demands along the height of dam D1 subjected to: (a) and (b) Imperial Valley (1940) ground motion; (c) and (d) Parkfield (1966) ground motion; (e) and (f) Loma Prieta (1989) ground motion; and (g) and (h) Saguenay (1988) ground motion.
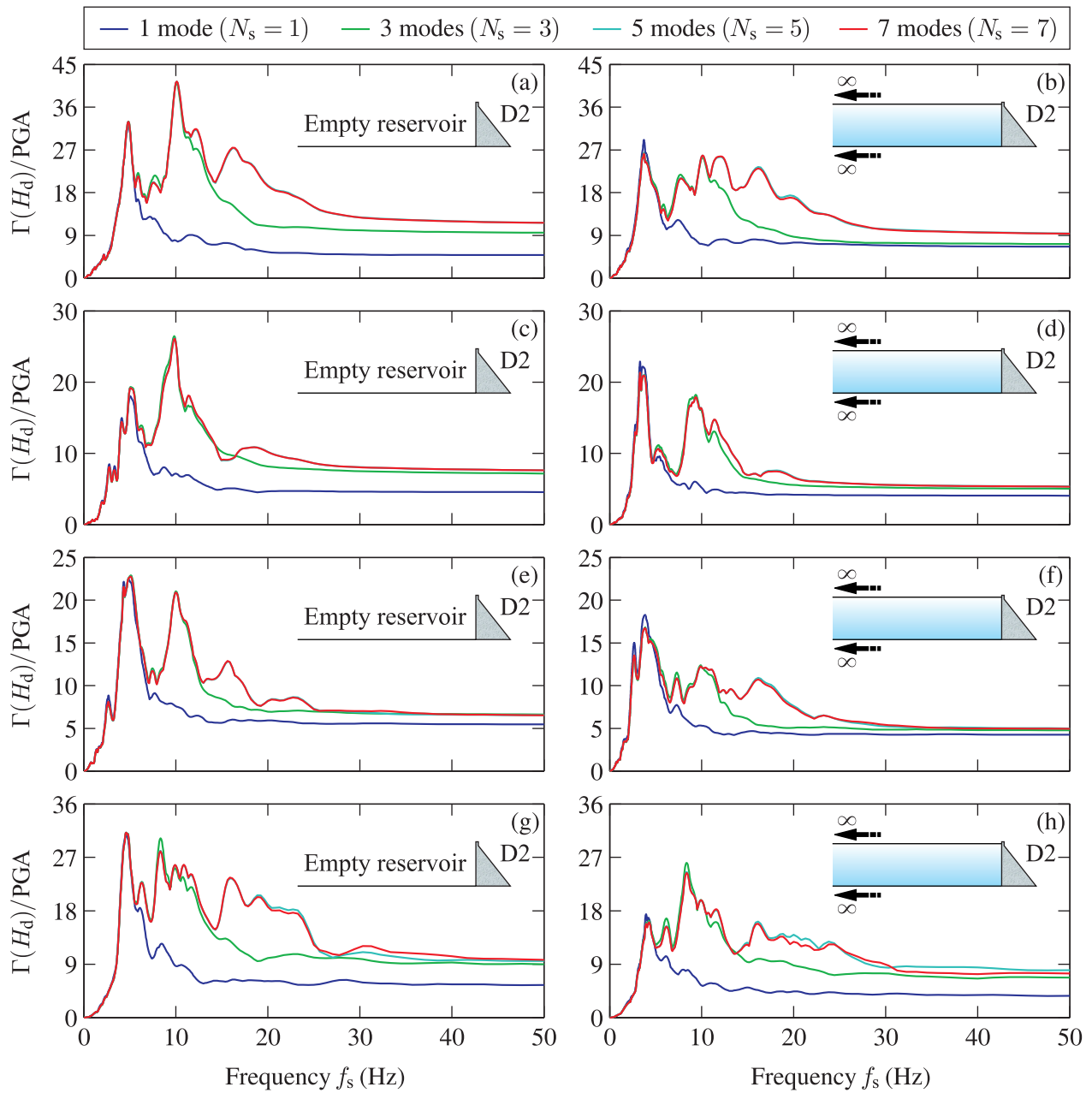
Figure 19. Effect of the number of structural modes included in the analysis on floor acceleration demands at the crest of dam D2 subjected to: (a) and (b) Imperial Valley (1940) ground motion; (c) and (d) Parkfield (1966) ground motion; (e) and (f) Loma Prieta (1989) ground motion; and (g) and (h) Saguenay (1988) ground motion.
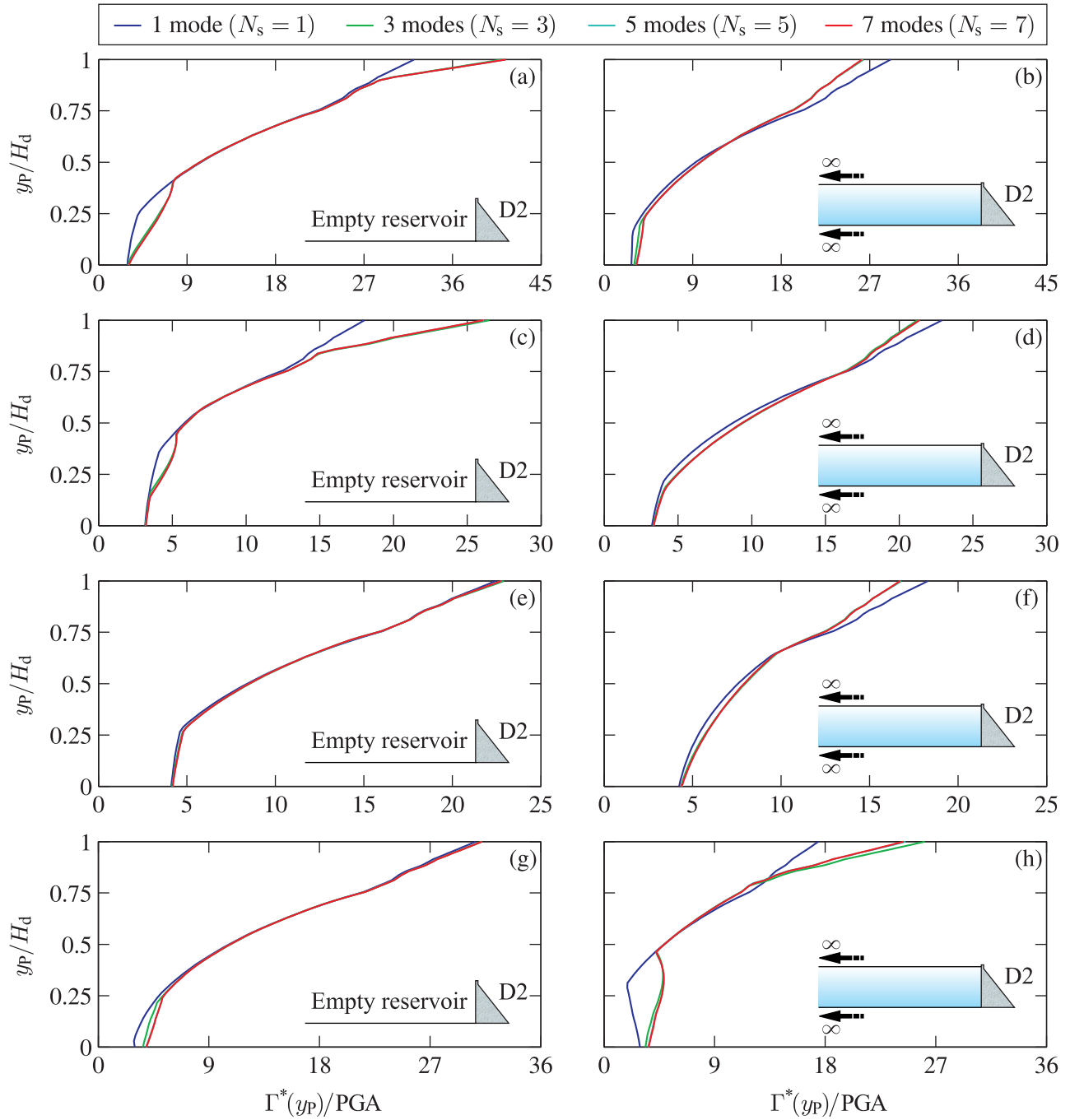
Figure 20. Effect of the number of structural modes included in the analysis on maximum floor acceleration demands along the height of dam D2 subjected to: (a) and (b) Imperial Valley (1940) ground motion; (c) and (d) Parkfield (1966) ground motion; (e) and (f) Loma Prieta (1989) ground motion; and (g) and (h) Saguenay (1988) ground motion.
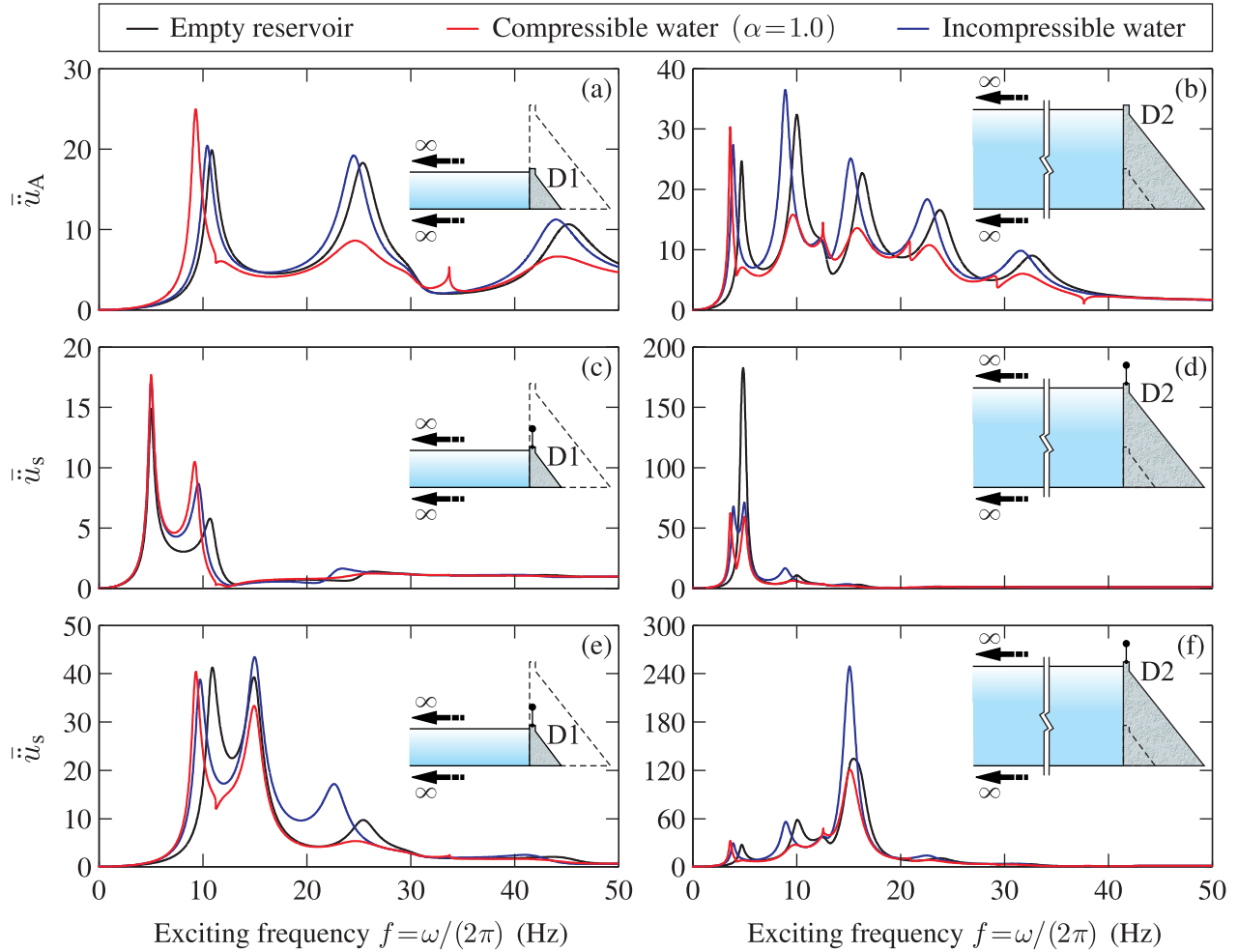
Figure 21. FRFs and FFRFs of the horizontal accelerations considering empty, compressible and incompressible water reservoirs: (a) FRF for dam D1; (b) FRF for dam D2; (c) FFRF for 5 Hz-system at the crest of dam D1; (d) FFRF for 5 Hz-system at the crest of dam D2; (e) FFRF for 15 Hz-system at the crest of dam D1; (f) FFRF for 15 Hz-system at the crest of dam D2.